Title

Evaluating the effectiveness of in-situ non-invasive photophysical characterization methods for distinguishing indigo from other blue colorants

Author

Salas, Megan Elizabeth

Publication Date

2020

Peer reviewed|Thesis/dissertation

UNIVERSITY OF CALIFORNIA

Los Angeles

Evaluating the effectiveness of in-situ non-invasive photophysical characterization methods for distinguishing indigo from other blue colorants

A thesis submitted in partial satisfaction

of the requirements for the degree Master of Arts

in Conservation of Archaeological and Ethnographic Materials

by

Megan Elizabeth Salas

2020

ABSTRACT OF THE THESIS

Evaluating the effectiveness of in-situ non-invasive photophysical characterization methods for distinguishing indigo from other blue colorants

by

Megan Elizabeth Salas

Master of Arts in Conservation of Archaeological and Ethnographic Materials

University of California, Los Angeles, 2020

Professor Ioanna Kakoulli, Chair

Indigo, a blue colorant extracted from the leaves of several plants found throughout the world, has a long history of use, stretching back to the third millennium BCE. In the last decades, its identification on cultural heritage materials was achieved through Raman spectroscopy and fiber optics reflectance spectroscopy (FORS). In recent years, an imaging method called multiband reflectance imaging subtraction (MBRIS) has been introduced to the cultural heritage field to identify and map indigo. As with FORS, this method takes into consideration the electronic properties of indigo and its optical behavior in the visible range. More specifically, this method is based upon the subtraction of two broadband images, one taken at the maximum absorption and a second one at the inflection point of the steep reflectance. This MA research reexamines the potential for the unbiased characterization of indigo using multiband reflectance imaging, reflectance and fluorescence spectroscopy, and hyperspectral imaging (HSI). Reference blue colorants as well as archaeological and ethnographic objects were analyzed using the aforementioned techniques. This MA research critically reviews the strengths of the techniques currently used for the characterization of indigo and compares how data are affected by factors such as concentration of the analyte and

substrate. The extent to which the fluorescence of indigo can be used for its differentiation amongst other blue colorants for materials characterization is also explored. While FORS was able to unequivocally differentiate between indigo and the other blue colorants, the MBRIS method was not. Case studies revealed that the MBRIS can provide false-positives and may not be well-equipped to map indigo present in high concentrations. The bandpass filters used in the MBRIS method are too broad to provide unbiased identification of colorants. Greater differentiation of powdered pigments in powder form was achieved with a new method of generating false-color images that utilizes principles of MBRIS. HSI spectroscopy, combined with trichromatic false-color imaging processing has shown promising results in terms of data visualization. The fluorescence of indigo could not be detected in solid samples with the spectroscopy setups used in this study; this suggests the emission is likely too weak to be captured by luminescence imaging techniques used in the cultural heritage field.

The thesis of Megan Elizabeth Salas is approved.

Christian Fischer

Laurent Pilon

Ioanna Kakoulli, Committee Chair

University of California, Los Angeles

2020

Table of Contents

List of Figures

List of Tables

Acknowledgements

I want to thank several people that have supported me throughout this project. First, I would like to thank my advisor Ioanna Kakoulli for sharing her expertise and knowledge during this process. I would also like to thank my committee members Professors Christian Fischer and Laurent Pilon for their help and feedback. I would also specifically like to thank: Christian de Brer of the Fowler Museum for facilitating my access to the museum objects that were part of this study; Roxanne Radpour for her guidance and assistance in the early phases of this project; and Ignacio Martini for his help in the MIC lab. Additionally, I want to thank everyone else at the UCLA/Getty Program, including Professor Ellen Pearlstein, Vanessa Muros, and all of my classmates.

1. Introduction

Indigo is a blue colorant that has a long history of use as a dye across the world (Seixas de Melo, Moura, and Melo 2004) and is still widely used today (Blackburn, Bechtold, and John 2009). For millennia, indigo was extracted from plants and used as a colorant on paintings and textiles. Since the early 20th century, chemically synthesized has replaced plant-sourced indigo for widespread use as a colorant, most notably as the dye used for blue jeans (Clark, Cooksey, and Daniels 1993). Indigo has been the subject of study in the fields of biochemistry, physical chemistry, spectroscopy, archaeometry, conservation science, and conservation imaging. Given its long and widespread use as a colorant, indigo is commonly found as part of material cultural heritage and thus is often the subject of analytical investigation by cultural heritage professionals.

2. Research objectives

This research explores and evaluates the effectiveness of selected in-situ non-invasive photophysical and imaging characterization techniques for distinguishing indigo from other blue colorants. Technical investigations of indigo are not new to the field of cultural heritage conservation and conservation science (Aceto et al. 2014; Miliani, Romani, and Favaro 1998; Leona et al. 2004; Seixas de Melo, Moura, and Melo 2004). The two major foci in this MA research are: 1) the reexamination and evaluation of the reliability of the multiband reflectance image subtraction (MBRIS) method (Webb, Summerour, and Giaccai 2014) for indigo identification, mapping, and differentiation from other blue colorants; and 2) the reassessment of the luminescence properties of indigo (Clementi et al. 2009; Romani et al. 2010) and the limitations for its detection using fluorescence spectroscopy. In order to have a baseline for the investigations, the photophysical properties of pure indigo and other blue colorants, and indigo applied on a variety of substrates and in different concentrations were analyzed using fiber

optics reflectance spectroscopy (FORS) and hyperspectral imaging spectroscopy (HSI).

3. Background and Fundamentals

3.1 Historical overview

Indigo can be extracted from the leaves of several plants found throughout the world: *Indigofera tinctoria* in Tropical Asia, *Isatis tinctoria* in Europe, *Polygonum tinctorium* in Japan and Southeast Asia, and *Indigofera suffruticosa* and *Indigofera arrecta* in Central and South America (Clark, Cooksey, and Daniels 1993; Blackburn, Bechtold, and John 2009). The chemically identical indigo ($C_{16}H_{10}N_2O_2$) compound can be obtained from each of these distinct plants (Clark, Cooksey, and Daniels 1993). *Indigofera tinctoria* is commonly referred to as the indigo plant, while *Isatis tinctoria* is known as the woad plant (Clark, Cooksey, and Daniels 1993; Degani, Riedo, and Chiantore 2015).

Ancient Egyptian textiles provide evidence of indigo's use as a dye dating back to at least the 3rd millennium BCE (Balfour-Paul 1998; Blackburn, Bechtold, and John 2009). In *The Natural History,* Pliny the Elder, Roman naturalist and author, describes "indicum," a costly colorant that comes from India that appears black in powder form, but deep blue when diluted in water (Pliny the Elder, Book 35, chapter 27); it is generally accepted that Pliny is describing the product of *Indigofera tinctoria* that Pliny is describing (Clark, Cooksey, and Daniels 1993). Pliny's accounts refer to indigo as a 'pigment' which was imported to Rome from India and is used by painters (Pliny the Elder, Book 33, chapter 57). Pliny also describes medical uses for indicum (Pliny the Elder, Book 35, chapter 27), but does not describe using it to dye cloth.

Indigo from woad has been identified on textiles from the Iron Age (ca. 700 BCE) (Balfour-Paul 1998). By the 17th century, imported indigo from India had become more popular than producing indigo from woad in western Europe (Clark et al. 1993). In the 17th century, indigo from *Indigofera tinctoria* began to be used as a dye in Western Europe when Dutch

traders made contact with India (Clark et al. 1993; Perkin 1900). Importation of indigo from India to Europe dramatically increased after 1602 (Clark et al. 1993; Perkin 1900). Importation of indigo from India was met with resistance by European woad growers, as the amount of dye that could be extracted from the *Indigofera tinctoria* was much greater than the amount that could be obtained from woad (*Isatis tinctoria*) (Clark et al. 1993; Perkin 1900). By 1900, imported indigo had surpassed woad as the major source of the dyestuff (Perkin 1900).

A historical account of indigo production in India describes that, in order to obtain the colorant from *Indigofera tinctoria*, the plants (leaves, pods, and stalks) are cut up and soaked in water to allow fermentation to occur over 10-15 hours (Perkin 1900; Degani, Riedo, and Chiantore 2015). Then, the vat is aerated by exposing it to oxygen in the air and agitating the liquid mechanically (Clark, Cooksey, and Daniels 1993; Degani, Riedo, and Chiantore 2015). The vat is then allowed to settle and the supernatant liquid is removed and the result is precipitated blue sludge, which is purified by heating and filtering; then it is dried out to produce the blue indigo powder (Clark, Cooksey, and Daniels 1993; Degani, Riedo, and Chiantore 2015). It is this blue solid that can be easily exported and then ground up for use as a colorant (Balfour-Paul 1998). Another method of production also includes making the vats basic by adding alkalis or ammonia (Perkin 1900). Extracting the indigo from the plant, as described above, is not the only way to dye with indigo; dyeing can occur in the same pot as the fresh or fermented plant material (Balfour-Paul 1998).

German chemist Adolf von Baeyer determined the chemical structure of indigo in 1883 (Baeyer and Drewsen 1882; Clark, Cooksey, and Daniels 1993; Perkin 1900) and was the first to synthesize it; chemically synthesized indigo became available on the market later that decade (Blackburn, Bechtold, and John 2009). Synthesized indigo on average contained a much larger amount of the primary color-producing molecule indigotin (discussed in following section) (Perkin 1900). By the turn of the 20th century, the synthetic production of indigo was poised to

outpace the production of indigo from natural sources (Perkin 1900) and import of indigo from India to Europe dramatically decreased (Clark, Cooksey, and Daniels 1993).

3.2 Chemistry of indigo

Chemically, “indigo” consists of varying amounts of several organic molecules. The primary molecule responsible for the blue color is indigotin (Figure 1a) (*trans*-indigo) (Degani, Riedo, and Chiantore 2015) or 2-(1,3-dihydro-3-oxo-2H-indazol-2-ylidene)-1,2-dihydro-3H-indol-3-one (Blackburn, Bechtold, and John 2009). In many contexts, this molecule is simply referred to as “indigo” (Figure 1b). However, there are other minor products that form during production that can be present in varying amounts in the final indigo product; these include *cis*-indigo and indirubin (also known as *trans*-indirubin, a red isomer of indigotin) and the *cis* forms of indigotin and indirubin (Degani, Riedo, and Chiantore 2015).

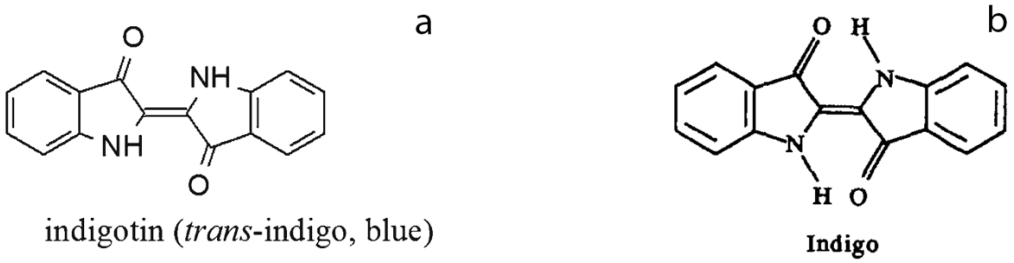

Figure 1. Chemical structure of indigo.
a) Indigotin, the primary molecule in indigo. Figure courtesy of Degani, Riedo, and Chinatore 2015, fig. 1 excerpt, page 1696 b) Indigotin molecule labelled as “indigo.” Figure courtesy of Clark, Cooksey, and Daniels 1993, Scheme 1 excerpt, page 196.

Indigotin and the isomers described above are produced when indoxyl molecules couple (Degani, Riedo, and Chiantore 2015) (Figure 2). The indoxyls are produced during the fermentation of the plant material (Clark, Cooksey, and Daniels 1993; Degani, Riedo, and Chiantore 2015). Depending on the species of plant, the molecules that precede the indoxyls (called indigo precursors) can differ; in *Indigofera* species and *Polygonum tinctorum,* indigotin comes from the indoxyl glycoside indican (Clark, Cooksey, and Daniels 1993; Degani, Riedo, and Chiantore 2015). Indican converts to an indoxyl via fermentation (Clark, Cooksey, and

Daniels 1993) or enzymatic hydrolysis (Degani, Riedo, and Chiantore 2015); then, two of these indoxyls couple to produce indigotin or one of its isomers. In the woad plant (*Isatis tinctoria*), isatan B is the major indigo precursor and indican is a minor contributor (Degani, Riedo, and Chiantore 2015).

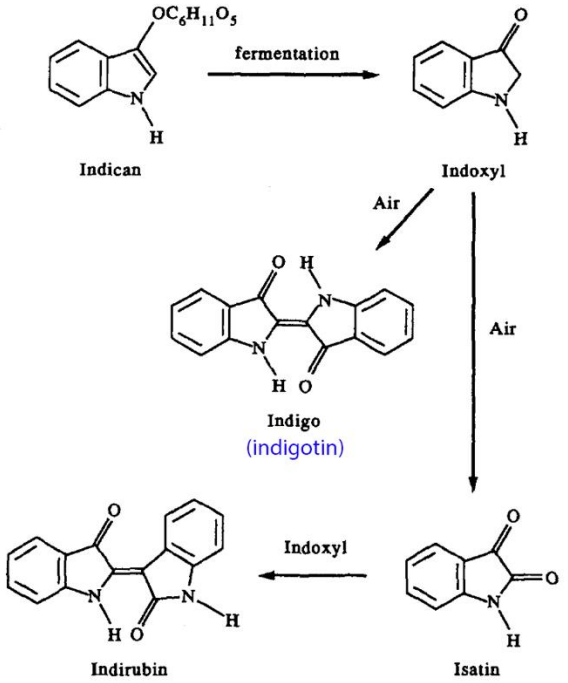

Figure 2. Conversion of indican precursor to indigotin with side reaction showing formation of indirubin.
Figure courtesy of Clark, Cooksey, and Daniels 1993, Scheme 1, page 196, with added annotation in blue.

Once the colorant has been extracted from the plant material via the above processes, it can be used as a dye. Indigo is a vat dye, which means that it must be reduced in order to become soluble in water (Clark, Cooksey, and Daniels 1993) (Figure 3). The oxidized (or keto) form of indigotin contains two carbonyl groups that can be reduced with a reducing agent plus alkali (Figure 3a); the reduced, water-soluble form is referred to as the *leuco* indigotin form (Figure 3b) (Blackburn, Bechtold, and John 2009; Clark, Cooksey, and Daniels 1993; Seixas de Melo, Moura, and Melo 2004). *Leuco*-indigo, (2,2'-bi-1H-indole)-3,3'-diol (Blackburn, Bechtold, and John 2009), is off-white to pale yellow (Clark, Cooksey, and Daniels 1993) and has commonly been called "indigo-white" (Perkin 1900). Addition of an alkalizing agent to the vat

increases the water-solubility of the *leuco* species (now disodium-(2,2'-bi-1H-indole)-3,3'-diolate) (Blackburn, Bechtold, and John 2009). Historically, common alkalizing agents included plant ash (Balfour-Paul 1998). The alkaline *leuco*-indigo is attracted to cellulosic fibers through Van der Waals and dipolar forces (Blackburn, Bechtold, and John 2009).

Traditionally, reduction of the indigo vat proceeded due to bacterial fermentation (Blackburn, Bechtold, and John 2009). During the 19th century, chemical alternatives began to be employed to induce reduction (Blackburn, Bechtold, and John 2009); the most common reducing agent was sodium hydrosulphite (sodium dithionite) (Blackburn, Bechtold, and John 2009). The use of hydrosulphite vat allowed reduction to occur more quickly than fermentation (Blackburn, Bechtold, and John 2009). Since the 20th century, sodium hydrosulphite is the main reducing agent used in industrial vat dyeing (Blackburn, Bechtold, and John 2009).

When the textile is removed from the vat, the indigo in the fibers comes into contact with oxygen in the air and the *leuco* form oxidizes back to the blue keto form (Blackburn, Bechtold, and John 2009; Degani, Riedo, and Chiantore 2015). The insoluble indigo becomes mechanically trapped within the fiber structure of the textile and thus does not get washed out (Blackburn, Bechtold, and John 2009).

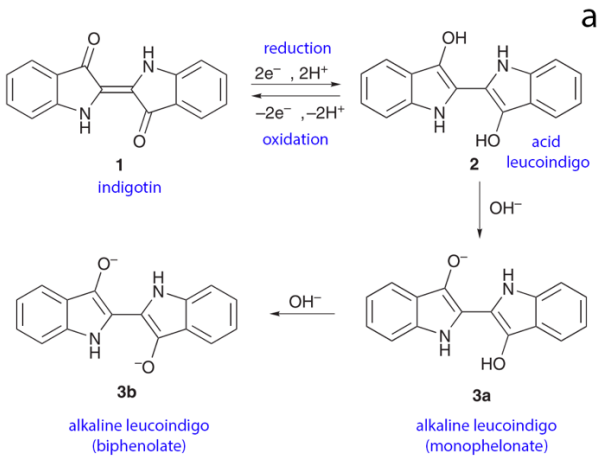

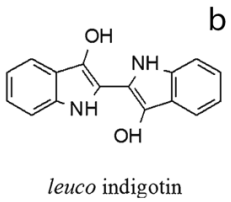

Figure 3. Processes that occur in the indigo vat.
a) 1: indigotin (keto form) is reduced to 2: acid *leuco*-indigo (enol form). Addition of alkalizing agent to converts molecule to 3a: monophenolate ionic form of alkaline leuco-indigo. Further addition of alkali causes formation of 3b: biphenolate form.
Figure courtesy of Blackburn, Bechtold, and John 2009, Scheme 1, page 193, with added annotations in blue.
b) Structure of *leuco* indigotin. Figure courtesy of Degani, Riedo, and Chiantore. 2015, fig. 1 excerpt, page 1696.

3.3 Photophysical properties of indigo

Indigo is a deep blue solid powder that is insoluble in water as well as many other common solvents (Clark, Cooksey, and Daniels 1993). Indigo is soluble in dimethylsulfoxide (DMSO), dimethylformamide (DMF), dioxane, and 2-methyltetrahydrofuran (2-MeTHF) (Pina et al. 2017; Seixas de Melo, Moura, and Melo 2004).

The main chromophores responsible for the blue color of indigotin are the double bond that joins the two rings as well as the carbonyl and nitrogen groups (Seixas de Melo, Moura, and Melo 2004; Degani, Riedo, and Chiantore 2015). Indigo is known as a light-stable material; this photostability has been attributed to excited-state proton transfer (specifically single proton transfer) (Seixas de Melo, Moura, and Melo 2004; Pina et al. 2017).

3.3.1 Indigo in the solid state

The reflectance spectrum of indigo (Table 1, Figure 4) in the solid state is characterized by an asymmetrical reflectance peak (λ_{ref}max) in the violet region (~420 nm) (Aceto et al. 2014), an asymmetric absorption band between 420 nm and 730 nm (Leona et al. 2004) with a maximum absorption (λ_{abs}max) at ~660 nm (Wyman and Weinstein 1956; Monahan and Kuder 1972; Leona et al. 2004; Angelini et al. 2010; Aceto et al. 2014; Cosentino n.d.), followed by a steep rise to high reflectance that begins to decrease around ~1500 nm (Aceto et al. 2014; Delaney et al. 2005). Spectral features of indigo are best resolved when a small amount of the colorant is dispersed in an inert material like barium sulfate to reduce the absorption (Figure 4b) (Leona et al. 2004). The absorption band of indigo in the visible region is due to electronic π-π* transitions from the highest occupied molecular orbital (HOMO) to the lowest unoccupied molecular orbital (LUMO) (Leona et al. 2004). In the NIR, indigo exhibits secondary absorptions at ~1139, ~1670, ~2060, ~2160, ~2280, ~2380, and ~2407 nm (Tsiantos et al. 2012; Fischer 2020) (Figure 4d).

In the field of cultural heritage, indigo is present as a dye on a fiber substrate or as a pigment mixed with a binder. Analysis of a reference sample of indigo on wool measured the maximum absorption to be ~660 nm (Angelini et al. 2010). Analysis of a reference sample prepared according to traditional illumination manuscript methods (organic binder on parchment) (Aceto et al. 2014) revealed that the indigo sample also had a maximum absorption at 660 nm (Figure 4c). According to Miliani et al. 1998, the maximum absorption of indigo when mixed with linseed oil and spread on canvas is red-shifted to 700 nm (Miliani, Romani, and Favaro 1998). Based on the technical data of the pigment from Sigma-Aldrich (Sigma-Aldrich n.d.), the synthetic indigo powder has a maximum absorption at 602 nm, although no specification is given whether this means in solution or as a powder.

Table 1. Summary of photophysical studies of indigo.

Publication	**Sample**	**Wavelength of maximum reflectance in visible region λ_{ref}max (nm)**	**Wavelength of maximum absorption λ_{abs}max (nm)**
Aceto et al. 2014	Indigo mixed with egg white/gum arabic on parchment	blue/violet region ~425	660
Angelini et al. 2010	Indigo on wool	~425	~660
Leona et al. 2004	Indigo mixed with barium sulfate	420	660
Miliani, Romani, and Favaro 1998	Indigo mixed with linseed oil, on canvas	--	700
Monahan and Kuder 1972	Indigo	--	668 (crystalline) 640 (amorphous)
Wyman and Weinstein 1956	Indigo in potassium bromide pellet	--	660
Sigma-Aldrich technical data (Sigma-Aldrich n.d.)	Indigo	--	602

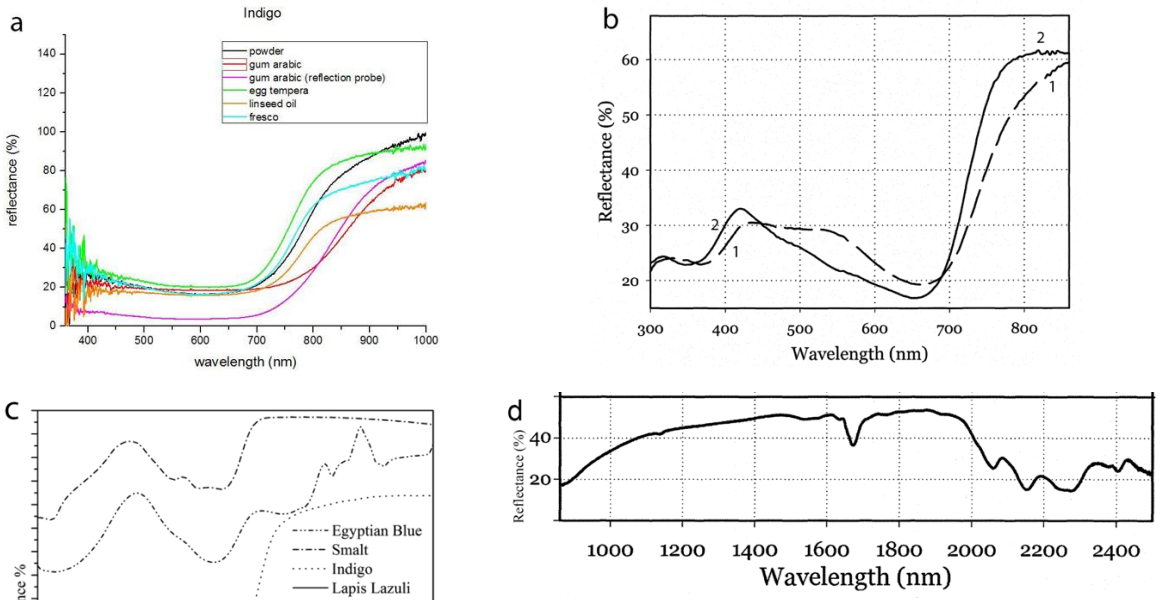

Figure 4. Reflectance spectra of indigo.
a) FORS spectra of indigo in different binders. Figure courtesy of Cosentino, https://chsopensource.org/fors/#BLUES.
b) Reflectance spectra of (1) modern Maya blue and (2) indigo (17% in barium sulfate). Figure courtesy of Leona et al. 2004, fig. 4, page 45.
c) Reflectance spectra of blue colorants measured on parchment; binder either egg white or gum arabic. Figure courtesy of Aceto et al. 2014, fig. 9, page 1495.
d) NIR spectrum for indigo.
Figure courtesy of Leona et al. 2004, fig. 3 excerpt, page 44.

There has been limited research exploring the fluorescence behavior of indigo as a potential identification tool (Table 2) (Miliani, Romani, and Favaro 1998; Clementi et al. 2009; Romani et al. 2010). Clementi et al. 2009 examined the use of in-situ fluorimetry to explore the organic colorants on Italian Renaissance tapestries (Clementi et al. 2009). In their study, the fluorescence of indigo was measured with a portable fluorimeter; when areas of the tapestry believed to contain indigo were excited with ultraviolet (UV) illumination (λ_{exc} = 350 nm) or in the visible (λ_{exc} = 600-650 nm), a weak photon emission at a longer wavelength (fluorescence) was observed at λ_{em}max = 750 nm (Figure 5).

This fluorescence at ~750 nm is weak (Clementi et al. 2009). By examining the intensity of the photon emission at 750 nm, it was observed that this was weaker in areas where the

textile appeared to be darker blue; the authors suggest that this result is possibly due to the "self-absorption of the light emitted by the dye" (Clementi et al. 2009).

A photon emission at a wavelength $\lambda_{em}max$= 730 nm was also reported on a blue-colored area of the Book of Kells (pigment with gum arabic on parchment) (Romani et al. 2010); they report that this emission is consistent with known standards of natural indigo in gum arabic (Romani et al. 2010). The excitation wavelength was not specified.

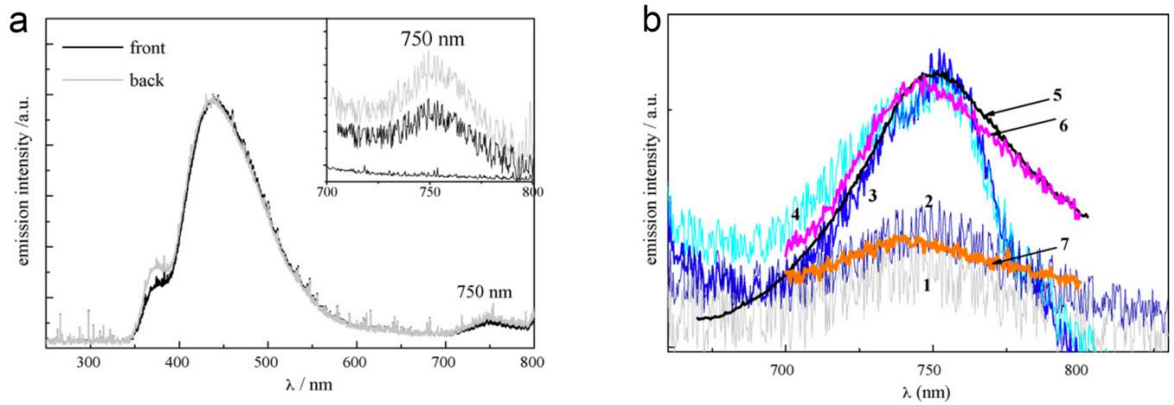

Figure 5. Emission spectra from blue areas of tapestries.
a) Emission spectra from a blue area of the textile Listra's Sacrifice (λ_{exc}=350 nm). Insert: detail of spectra collected in the same area of textile (λ_{exc}=650 nm) showing weak emission around 750nm attributed to the fluorescence of indigo.
b) Emission spectra from blue areas of Earthquake in Filippi (λ_{exc}=600-650 nm): soldier's shirt (1); grate (2); sky (3); soldier's corace (4). Emission spectrum of solid indigo (5), silk dyed with indigo (6) and wool dyed with indigo (7).
Figures courtesy Clementi et al. 2009. a) fig. 8, page 2060 b) fig. 9, page 2061

The aforementioned work built off of previous studies of the photophysical properties of indigo and indigo used as a paint mixed with a binder (Miliani, Romani, and Favaro 1998). When mixed with linseed oil and spread on canvas, the maximum emission occurred at 750 nm; the excitation wavelength was not specified (Miliani, Romani, and Favaro 1998). These authors posit that the red shift of the emission when applied on canvas could be due to the interaction of the molecule with the binder or to intermolecular aggregation (Miliani, Romani, and Favaro 1998).

Table 2. Summary of indigo fluorescence studies.			
Publication	**Object of study**	**Excitation wavelength λ_{exc} (nm)**	**Emission wavelength λ_{em}max (nm)**
Romani et al. 2010	Pigment in gum Arabic binder on parchment (Book of Kells)	Unspecified	730
	Blue area of Renaissance tapestries (*Listra's Sacrifice & Earthquake in Filippi)*	350	750
Clementi et al. 2009	Blue area of Renaissance tapestry (*Listra's Sacrifice)*	350 and 600-650	750
	Blue area of Renaissance tapestry (*Earthquake in Filippi)*	600-650	750
	Green areas of tapestries	350	750
Miliani, Romani, and Favaro 1998	indigo in 1,2-dichloroethane solution	~600	~650, 720
	Indigo mixed with linseed oil and spread on canvas	Unspecified	~750

3.3.2 Indigo in solution

The absorption and reflectance properties of indigo have been studied with the molecule in solution (Table 3) (Wyman and Weinstein 1956; Seixas de Melo, Moura, and Melo 2004; Pina et al. 2017). The main absorption is documented as occurring at shorter wavelengths (~601-619 nm) when the molecule is in solution compared to the solid state (Wyman and Weinstein 1956; Seixas de Melo, Moura, and Melo 2004). The solvent used can shift the main absorption maximum (Pina et al. 2017) with more polar solvents causing a red shift (Miliani, Romani, and Favaro 1998).

The fluorescence of indigo in solution has also been studied. When indigo in solution (1,2-dichloroethane) was excited at ~600 nm, a maximum emission at 650 nm was recorded with a secondary emission at 720 nm (Miliani, Romani, and Favaro 1998). The fluorescence quantum yield—defined as the ratio of the molecules that fluoresce to the number of excited molecules (Matarazzo and Hudson 2015)—was 0.001 (Miliani, Romani, and Favaro 1998).

In more recent studies, the fluorescence of indigo in solution was generally observed at ~650 nm (Pina et al. 2017; Seixas de Melo, Moura, and Melo 2004). In the study by Pina et al., the fluorescence quantum yield was measured to be between 0.0019 to 0.0025 depending on the solvent (Pina et al. 2017). Thus, contrary to early studies that asserted that indigo exhibited

no fluorescence (Kobayashi and Rentzepis 1979), indigo does exhibit weak fluorescence (Seixas de Melo, Moura, and Melo 2004; Miliani, Romani, and Favaro 1998). By comparison, the pigment Egyptian blue, which exhibits intense visible-induced near-infrared (NIR) fluorescence has a fluorescence quantum yield of 0.11 (Accorsi et al. 2009; Verri 2009). The weak nature of indigo's fluorescence is due to the small energy difference between the lowest singlet excited state (S1) and the ground state (S0) (Seixas de Melo, Moura, and Melo 2004); this small energy difference means that a nonradiative decay pathway is favored over a radiative decay pathway (Seixas de Melo, Moura, and Melo 2004).

Table 3. Summary of studies of indigo in solution.

Publication	**Experimental details**	**λ_{abs}max (nm)**	**λ_{exc} (nm)**	**λ_{em}max (nm)**	**Fluorescence quantum yield Φ_F**
Pina et al. 2017	Sigma-Aldrich indigo in various solvents	DMSO: 619 Dioxane: 601 DMF: 610 2-MeTHF: 602	560	DMSO: 665 Dioxane: 637 DMF: 653 2-MeTHF: 631	DMSO: 0.0019 Dioxane: 0.0025 DMF: 0.0023 2-MeTHF: 0.0019
Seixas de Melo, Moura, and Melo 2004	Sigma-Aldrich indigo in DMF	610	535	653	0.0023
Miliani, Romani, and Favaro 1998	Synthetic indigo in 1,2-dichloroethane	603	~600	650	0.001
Monahan and Kuder 1972	Indigo (J.T. Baker) in solution	Chloroform: 604 Ethanol: 610	--	--	--
Wyman and Weinstein 1956	Indigo (commercially available) in chloroform	604	--	--	--

Other research has focused on the photophysical properties of the *leuco* (or reduced) form of indigo (Seixas de Melo, Moura, and Melo 2004). The *leuco* form was prepared by adding sodium dithionate and sodium hydroxide to the dye in solution (Seixas de Melo, Moura, and Melo 2004). The maximum absorption of the *leuco* species in DMF was at ~442 nm (Seixas de Melo, Moura, and Melo 2004); the *leuco* form exhibits stronger fluorescence, with a maximum emission at 523 nm in DMF (Seixas de Melo, Moura, and Melo 2004). The fluorescence quantum yield was measured to be 0.348 compared to 0.0023 for the keto form

(Seixas de Melo, Moura, and Melo 2004). This stronger fluorescence is likely due to a greater difference in structure and energy level between the lowest singlet excited state and the ground state of the *leuco* form (Seixas de Melo, Moura, and Melo 2004).

3.4 Techniques and methods for the characterization of indigo

The most common method of identification for indigo, as well as other dyes, is chromatography, specifically high pressure liquid chromatography with mass spectrometry (HPLC/MS) (Clementi et al. 2009). This method of characterization involves physically separating the dye into its components and then identifying these components (Maugard et al. 2001); this method is minimally invasive and minimally destructive, meaning that it requires removal and consumption of a microsample. Gas chromatography-mass spectroscopy (GC/MS), another minimally invasive and destructive technique, has also been used to analyze indigo (Degani, Riedo, and Chiantore 2015).

Infrared spectroscopy is another method used to identify indigo. Leona et al. 2004 point out that a significant challenge in using techniques like Fourier transform infrared spectroscopy (FTIR) and GC/MS to identify indigo in works of art is that the dye is often present is a very low concentration and the signal from indigo is often overwhelmed by signals from other components present such as the binder, fiber substrate, or support (Leona et al. 2004).

Other techniques used to identify indigo are fiber optics reflectance spectroscopy (FORS) and Raman micro-spectroscopy (μRS) (Leona et al. 2004). These two techniques are better suited for the identification of indigo than FTIR and GC/MS because they are less likely to be overwhelmed by contributions from other types of materials present in a sample (Leona et al. 2004). Both Raman and FORS can provide information about the chemical makeup and structure of molecules. FORS is easily applied non-invasively and in-situ; Raman spectroscopy is typically conducted on samples removed from objects, but there are also portable instruments that allow non-invasive and in-situ analysis.

3.4.1 Multiband reflectance image subtraction (MBRIS)

Multiband reflectance image subtraction (MBRIS) is an imaging method that utilizes the absorption and reflectance properties of indigo in the visible and NIR using broad-band imaging and has been explored as a method to characterize indigo in cultural heritage (Webb, Summerour, and Giaccai 2014; Bradley et al. 2018; Kriss et al. 2019). The first publications of this technique utilized a digital single-lens reflex (DSLR) camera that had been modified to capture infrared radiation and had its color filter array (CFA) removed (Webb, Summerour, and Giaccai 2014). This camera was equipped with bandpass filters (with bandwidths in the hundreds of nanometers): 660 nm and 735 nm (Webb, Summerour, and Giaccai 2014). Two images were captured of the target, one with each bandpass filter. Imaging processing software like Adobe Photoshop was used to process the monochrome images; using the difference blending mode, one image is subtracted from the other. The resulting image visualizes the differences between the two original images because image subtraction is a method of detecting change between two images (Webb, Summerour, and Giaccai 2014; Jain 1989). The 660 nm bandpass filter captures indigo near its maximum absorption, while the 735 nm bandpass filter captures the transition from absorbance to reflection. Thus, in the grayscale images, the 660 nm image will show indigo as black and the 735 nm image will show indigo as white. When the images are subtracted from each other, the indigo areas will appear white because of the different behavior in the two images.

This technique provides a low-cost alternative to using specialized analytical equipment to identify indigo. Cameras sensitive to IR radiation are already owned by many conservation labs. Museum professionals that have experimented with this technique emphasize that it is a useful preliminary tool, but that the conclusive identification of indigo requires additional characterization techniques such as FORS, X-ray fluorescence (XRF), and Raman (Webb, Summerour, and Giaccai 2014; Bradley et al. 2018). Webb points out that MBRIS becomes more difficult to use as a characterization method when there are mixtures of materials or

materials with similar reflectance profiles to indigo being imaged (Webb, Summerour, and Giaccai 2014). The limitations of this technique have also been explored by conservators at the Brooklyn Museum (Kriss et al. 2019; Bradley et al. 2018), who noticed inconsistent results when the exposure of the images collected was changed (Bradley et al. 2018).

The main reason that users should take caution when using this technique is that it utilizes the reflectance spectrum of indigo and broad bandpass filters. Any colorant that exhibits a reflectance profile similar to that of indigo in the red to near infrared region (absorbs at ~660 nm and reflects at ~735 nm) will produce a similar MBRIS result.

4. Materials & Methods

Reference colorants in powder form, mockups, as well as archaeological and ethnographic objects containing indigo, were analyzed using non-invasive techniques in order to compare and contrast the capabilities and limitations of these techniques. Reflectance characteristics of indigo were investigated with the following techniques: fiber optics reflectance spectroscopy (FORS), hyperspectral imaging (HSI) spectroscopy, and multiband reflectance image subtraction (MBRIS).

4.1 Materials

4.1.1 Powders reference samples of indigo and other blue colorants

Colorants in this research were analyzed in powdered form. Studying the colorants in this form ensures a high concentration of the colorant and eliminates any contribution from binding media or fiber substrate.

Reflectance spectra were collected on four indigo samples: Sigma-Aldrich (S-A) synthetic indigo, Botanical Colors (BC) organic natural indigo (from *Indigofera tinctoria*), indigo blue lake from Kremer Pigments, and pre-reduced indigo from a dyeing kit manufactured by Jacquard Products.

For comparison with indigo, the other blue colorants analyzed in powder form were: Maya blue, smalt standard grind, cobalt cerulean blue, cobalt blue medium, Lapis lazuli sky-blue, ultramarine blue light, Egyptian blue, Han blue fine 0-40 µm, phthalo blue, Heliogen® blue, Prussian blue, and azurite natural standard 0-120 µm. All were obtained from Kremer Pigmente.

Pigment powders were used as is or mixed with barium sulphate to dilute the concentration of the pigment. A hydraulic press and a mold were employed to prepare pellets of some of the powdered pigments (about 300-500 mg of powder).

4.1.2 Paint swatches

Due to the fact that indigo has been used as a pigment in painted media, paint swatches of indigo samples and other blue colorants were prepared as reference samples; the aim was to study the effect of binding media on the photophysical properties of these colorants. The binder employed was egg yolk in order to limit gloss. The substrate on which the swatches were painted consisted of carbon black dry pigment, calcium carbonate dry white pigment, and egg yolk. The colorants used for the paint outs were the same as those mentioned in the previous section.

4.1.3 Dyed fiber substrates

Due to indigo's wide use as a dye for textiles, studies were carried out on indigo in this form on a variety of fiber substrates. Plant-sourced (cotton) and animal-sourced (silk, wool, camelid) fibers were dyed with two different indigo sources, synthetic (S-A) and natural (BC), for various amounts of time. The effects of variables such fiber type, concentration, and source of indigo on the photophysical properties of the pigment were assessed.

The two indigo sources used for dyeing were the S-A synthetic and BC natural indigo. The fiber substrates were: woven cotton fabric (Organic Cotton, Aurora Silk), woven silk fabric (Silk Habutae, 8mm, Testfabrics, Inc.), woven wool fabric (Worsted Wool Challis, Testfabrics, Inc.), and camelid fiber yarn (Baby Llama Chunky, Cascade Fabrics).

For each indigo type, two small vats were prepared following the procedure available through the vendor Botanical Colors (“Indigo Instructions”). These consisted of 1:2:3 (by volume) parts indigo: alkalizing agent (calcium hydroxide): reducing agent (fructose and/or sodium hydrosulfite). For the preparation of the vats, indigo powder was mixed with warm (under 170°F) water to create a paste in a glass container. Then, one cup of warm water and the reducing agent were added and stirred until dissolved. The calcium hydroxide was then added and stirred until it is mostly dissolved. About two cups of warm water were added to the mix and the vat was covered. After about 30 minutes, three distinct layers developed: 1) a dark blue, iridescent surface with bubbles 2) a red-yellow liquid in the middle, and 3) a light green sediment at the bottom.

Following the formation of these three layers, the vat was stirred and poured into a larger vessel to more easily accommodate dyeing. The mixture was covered and allowed to settle until the sediment settled at the bottom. The pH of the vats was ~13. During dyeing and between dyeing sessions, when the reddish-yellow liquid started turning blue, more of the alkalizing and reducing agents were added (“Indigo Instructions” 2018). The Sigma-Aldrich vat was initially prepared using sodium hydrosulphite as a reducing agent because it was readily available in the lab. To balance this vat, fructose was added, in addition to more calcium hydroxide.

Prior to dyeing, small portions of fiber substrate were cut and allowed to soak in tap water for at least 30 minutes. The samples were then suspended in the vat liquid (not allowed to sink to the bottom) for varying amounts of time and then allowed to oxidize in the air upon removal from the vat. Samples that underwent multiple dyeing processes were allowed to oxidize overnight before being dyed again. After fully oxidizing and drying, the samples were rinsed to remove unbound indigo. The dyeing times refer to how long the sample was submerged in the vat. There were a total of six dyeing times: 30 seconds, 2 minutes (one dip), 2 minutes (two dips), 5 minutes (one dip), 5 minutes (two dips), and 10 minutes (one dip) plus 20 minutes (one dip).

4.1.4 Archaeological and ethnographic objects

In order to test how these methods of study applied to actual collection objects, several artifacts from the Fowler Museum at UCLA were selected and analyzed. Most of these objects were selected based on the likelihood that they contained indigo based on appearance, cultural association and chronology, and museum records. These objects include textiles from South America and Africa, ceramics from Central America, and paintings from Asia.

X90-271 is a partially dyed skein of yarn from Gori in western Mali, Africa (Fowler Museum, n.d.). According to museum records, the yarn is cotton and the dye is indigo (Fowler Museum, n.d.). Fowler museum records indicate that this object was purchased from the dyer Fatoumata Sacko as part of a joint project between the National Museum of Mali and the Fowler Museum UCLA Museum of Cultural History that focused on textile documentation and collecting (Fowler Museum, n.d.).

A textile fragment (X2011.31.34) from Peru, believed to be Pre-Colombian, was studied (Fowler Museum, n.d.). The textile contains three squares in a horizontal register and bordered on the top and bottom by red horizontal strips; in each square an animal (likely a canine) is depicted in profile stepping on another creature. Each square has a different color scheme: one is dark purple and orange, the central one is green and dark purple, and the third one is red and white. One side of the textile appears more faded than the other.

Two of the objects studied (X91-2253 and X91-2269) are Jaina-style figurines (McVicker 2012). Named after an island off of the coast of the Yucatan Peninsula where many of these objects were found, Jaina-style figurines are figural ceramic objects made by the Maya that usually represent humans or deities (McVicker 2012). Associated with burial practices, these figurines are typically made of orange clay and can contain applied pigments (McVicker 2012). The Fowler objects part of this study represent male figures, are hollow whistles, and contain areas of bright blue pigment (Fowler Museum, n.d., n.d.). The blue pigment was identified as likely being Maya blue based on its appearance and context. Maya blue is a pigment made of

indigo and clay (palygorskite) that was produced between the 6th-18th centuries CE in present-day Central America (Bernardino, Constantino, and De Faria 2018). The clay and dye are mixed and then fired (at 90-200°C) to produce a bright blue pigment (Bernardino, Constantino, and De Faria 2018). The use of FORS to discriminate between indigo and Maya blue () has been explored on Jaina-style figurines (Leona et al. 2004).

Finally, two Balinese paintings (X2006.19.1 and X.2006.19.2) were studied; a previous study of these works indicated the presence of blue colorants other than indigo on these canvas (cotton or linen) paintings. These paintings are from the village of Batuan in Bali, Indonesia and date to the first half of the 20th century (Fowler Museum, n.d., n.d.). One of the paintings (X2006.19.1) is by the artist Ida Bagus Oka (Fowler Museum, n.d.) and the other (X2006.19.2) is by Njm Kenjod (Fowler Museum, n.d.).

4.2 Methods

Three non-invasive imaging and spectroscopic characterization techniques were selected for this pilot research to address the goals and aims of this project: fiber optics reflectance spectroscopy (FORS), multiband reflectance image subtraction (MBRIS), and hyperspectral imaging spectroscopy (HSI). These were used to analyze reference samples, as well as cultural heritage artifacts containing indigo and other blue colorants.

4.2.1 Fiber Optics Reflectance Spectroscopy (FORS)

In the solid state, the best way to non-invasively characterize indigo is FORS (Leona et al. 2004; Leona and Winter 2001). Most commonly, a spectrophotometer from the ultraviolet to the short-wave infrared region is used (UV/Vis/SWIR). UV-vis spectroscopy is a type of electronic spectroscopy that provides information about molecules and compounds based on their behavior when excited with ultraviolet and visible electromagnetic radiation (Kakoulli et al. 2017; Fischer and Kakoulli 2018). In the visible region (~400-750 nm), these interactions are

manifested by the substance's color (Leona et al. 2004). In the NIR (~750-2500 nm), in addition to electronic processes, reflectance spectroscopy can detect characteristic combination and overtone bands related to the fundamental vibrational modes occurring in the mid-infrared (Fischer and Kakoulli 2018; Kakoulli et al. 2017).

In this research, a FieldSpec3® from Analytical Spectral Devices Inc. (ASD) was used. The spectral range of the instrument is 350 to 2500 nm with a resolution of 3 nm at 700 nm and 10 nm at 1400-2100 nm. Spectra were collected with a contact probe that is equipped with a halogen light source; the spot size is 8 mm in diameter. Calibration was performed against a white Spectralon® diffuse reflectance standard. Integration time was automatically determined by the instrument after optimization and white reference measurement. Data was processed with ViewSpec Pro™ software, also designed and manufactured by ASD.

To collect FORS spectra from the colorants in powder form, a thin layer (approximately 300 mg) of the powder was spread on a piece of weighing paper in an area needed to cover the diameter of instrument's spot size. The head was held pointing downward to the weighing paper by a clamp on a ring stand to limit movement; the distance between the glass of the FORS head and the sample was about ~1 mm to avoid contact with the powder, which could make cleanup difficult and potentially affect future measurements.

4.2.2 Multiband Reflectance Image Subtraction (MBRIS)

In this research, a Nikon D90 DSLR modified camera (with the hot mirror removed enabling the recording between ~350 and 1000 nm) was used. Interferential bandpass (BP) filters (660 nm and 735 nm) from Midwest Optical systems were used with this camera (Figure 6). Two Interfit® halogen 1000-watt lights were used for illumination. An image was captured with each filter; the exposure time of the 735 nm photo was adjusted to be slightly shorter than the 660 nm image to avoid overexposure (the typical settings were: 660 nm image collected with 1/20 exposure and 735 nm image collected with 1/30 exposure). An unmodified Nikon D90

was used to collect an RGB image with the same lighting conditions with an X-Rite ColorChecker Passport for calibration. This RGB image was color corrected using the ColorChecker Camera Calibration and Adobe Camera RAW software. This correction adjusted the color temperature, which was affected by the lights and the filters. This calibration was then applied to the images taken with the modified camera and bandpass filters. Then, the modified camera images were converted to grayscale in Camera RAW. These modified images were then opened in separate layers in Adobe Photoshop and the difference function was applied, giving the image subtraction final result.

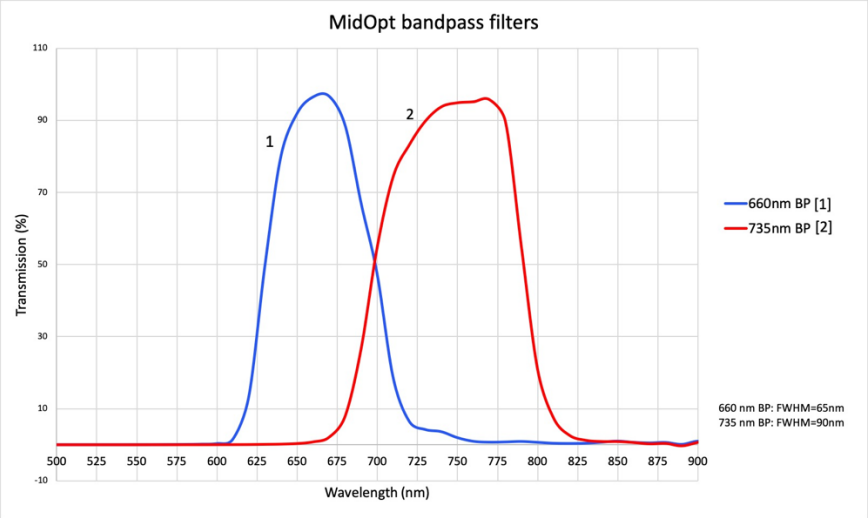

Figure 6. Transmissions of Midwest Optical bandpass filters used.
Data points are based on specifications provided by Midwest Optical.

In order to achieve a greater level of visual differentiation, a new approach was tested. False-color images were made using three grayscale images: 1) the MBRIS result 2) the 660 nm BP image and 3) the 735 nm BP image. In Adobe Photoshop, the green and blue channels of the MBRIS result were replaced with the 735 nm and 660 nm BP images, respectively; the red channel was not altered.

4.2.3 Hyperspectral Imaging (HIS)

HSI was carried out with a Specim IQ portable hyperspectral camera that has a spectral range of 400-1000 nm and a spectral resolution of 7 nm. The camera has a CMOS detector and records 204 spectral bands. Default recording mode was used to collect data. The custom white

reference mode was used, in which the camera calibrates against a white reflectance standard for each imaging session and configuration. Illumination was provided by Interfit® halogen 1000W lamps.

4.2.4 Spectrophotometry to detect fluorescence

FORS (using the instrument and software previously discussed in 4.2.1) was employed to attempt to detect fluorescence of powder reference samples. The analyte was placed on weighing paper and illuminated with an alternative light source (the Mini-Crimescope® MCS-400 by SPEX Forensics) that enables broadband selection of excitation wavelength. The FORS probe was placed at a 45° angle from the sample and the probe at a 90° angle to the sample to maximize diffuse reflectance and minimize specular reflectance. The probe was blocked from the light source to limit obtaining reflectance signal.

Further experiments were performed at the UCLA Molecular Instrumentation Center (MIC), where the spectroscopy setup is equipped for measuring samples in solution; the goal of this work was to see whether the instrumentation could detect the emission.

Before attempting to measure the fluorescence of indigo in solution, measurements were done to determine the wavelength of maximum absorption. Absorbance measurements of solutions were prepared at 0.01% by weight concentration in DMSO, except for Maya blue, which was prepared at 0.02% by weight concentration in DMSO. This low concentration was decided upon to keep the solution dilute; preliminary tests revealed that more dilute solutions enabled better resolution of the fluorescence peak. These measurements were done with an Agilent 8453 UV-Visible Spectrophotometer and data was collected and processed with Agilent ChemStation software.

An Ocean Optics USB 2000 spectrometer, connected with fiber optic cables to a light source and cuvette cell holder, was used to measure fluorescence of the solutions. The spectrophotometer has a spectral range of 340 nm to 1020 nm; the spectral resolution is ~0.38

nm. The solution was placed in a cuvette, which was placed in a cuvette holder that enabled the fiber optic cables delivering the light source and the fiber optic cable connected to the detector to be positioned at a 90° angle relative to each other with the cuvette in between. The sample was excited with a yellow LED bulb (Stellar Net Inc.) with maximum emission at 590 nm; this bulb was selected because it was close to the range of greatest absorption for indigo but would not interfere with the expected signal at ~620 nm. Data was visualized and processed with Ocean Optics Spectra Suite software.

The Ocean Optics USB 2000 spectrometer was also used to conduct experiments on solid state samples. A sampling accessory placed on top of the powdered analyte delivered the yellow LED (590 nm) light source and held the detector probe at a 45° angle. A 600 nm long pass filter was used to cut out radiation from the light source.

5. Results and Discussion

5.1 Indigo and other blue colorants powder reference samples

5.1.1 FORS

FORS spectra were mainly investigated in the visible and NIR regions closest to the visible because as these regions contribute to the MBRIS result. In addition to the main absorptions in these regions, the inflection point of the major transition from absorption to reflectance is important as well. The inflection point (λ_{inf})—where the second derivative of the reflectance spectrum changes sign—provides an indication of at which wavelengths this transition occurs.

5.1.1.1 Indigo samples

While the S-A, BC, and Kremer samples were in the form of fine powders, the Jacquard indigo was in the form of larger grains. For this reason and due to the fact that the Kremer sample was identified as a lake pigment, the S-A and BC indigo samples were identified as the

most appropriate materials to use as reference points.

Measurements were collected on pure samples of S-A and BC indigo (Table 4). To better resolve the absorption bands (Leona et al. 2004), 10 w% mixtures of the pigment in barium sulfate were prepared and analyzed (Figure 7). The reflectance spectra collected on the S-A and BC indigo samples were very similar. The spectra showed a reflectance maximum in the visible at ~420 nm, followed by a broad absorption band with maximum absorption at ~660 nm, and then a steep transition to reflectance beginning ~685-690 nm, with an inflection point ~740 nm, an absorption at ~860 nm, and continued rise to reflectance until around ~1400 nm. These results demonstrate that there is little difference in the visible and near infrared regions between the synthetic indigo powder and the natural indigo powder. The absorption at ~860 nm has not been noted in published literature. Possible sources for this absorption include impurities in the indigo, but further analysis is needed for definitive attribution.

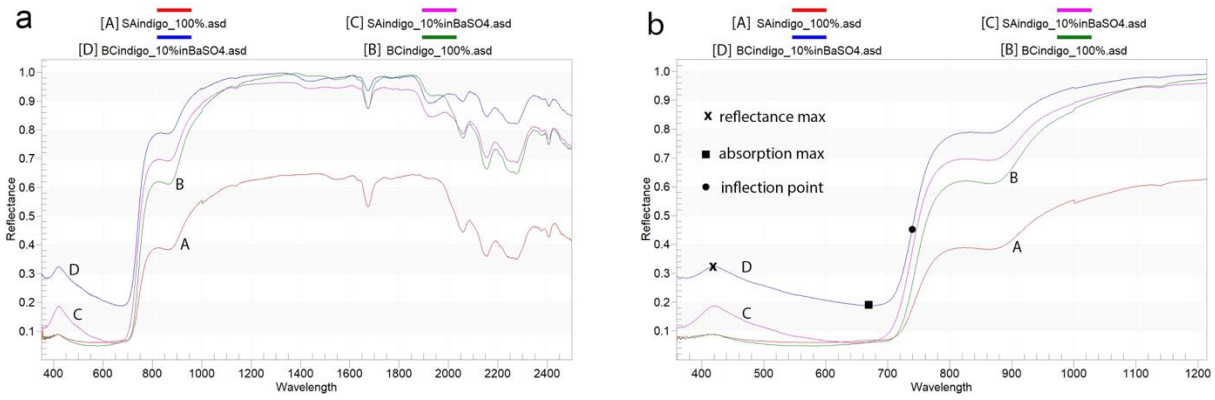

Figure 7. S-A and BC indigo samples reflectance spectra.
a) Reflectance spectra of 100% concentrations and mixed (10 w%) with barium sulfate. b) detail of reflectance spectra with features of [D] marked. For the rest of the spectra in this thesis, **x**= reflectance maximum, ■= absorption maximum, and •=inflection point.

There are some differences in the S-A and BC spectra that are better resolved with the first- and second-order derivatives of the reflectance spectra (Figure 8). The first-order derivative (Figure 8a) shows the slope of the reflectance spectrum at that point; thus, the first-order derivative passes through zero at the wavelength of maximum absorption. BC indigo

exhibits maximum absorption at 670 nm and the S-A Indigo exhibits maximum absorption at ~650 nm. The first-order derivative also reveals that the inflection points (visualized as maxima in the first derivative) are slightly shifted based upon whether the sample was 100% indigo powder or whether it was dispersed in barium sulfate. Examination of the second-order derivative allows precise identification of where these inflection points occur. In the second-order derivative (Figure 8b), inflection points are pass through zero; for the 10% mixtures, the inflection point is at ~738-740 nm, while for the 100% samples, this occurs at ~744-745 nm.

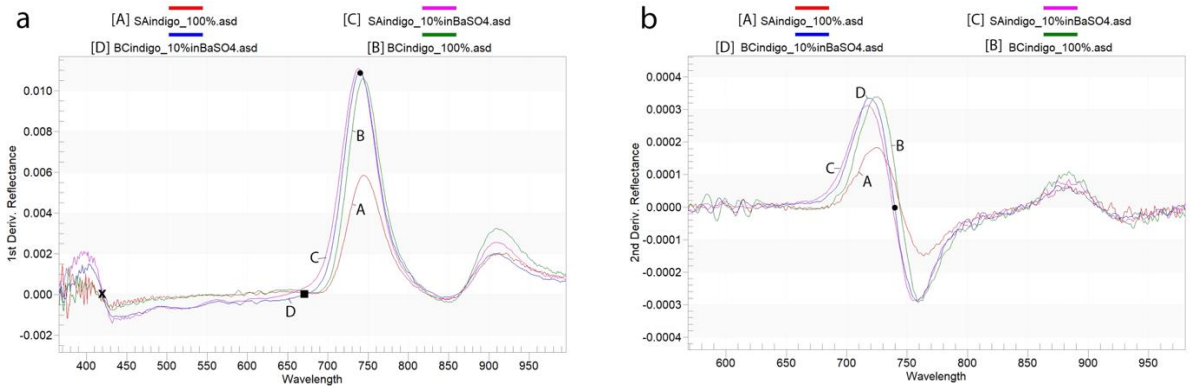

Figure 8. S-A and BC indigo samples, first- and second-order derivatives.
a) First-order derivative with features of [D] marked. λ_{abs}max for S-A is shorter than λ_{abs}max for BC indigo.
b) Second-order derivative with features of [D] marked. λ_{inf} of 10 w% mixtures occur at ~738-740 nm, while λ_{inf} of 100% indigo samples occur at ~744-745 nm.

The Jacquard indigo (10 w% in barium sulfate) produces a reflectance spectrum (Figure 9) with the following features: reflectance maximum at ~416 nm, maximum absorption at ~655 nm, an inflection point at ~726 nm, and an absorption at ~870 nm. Thus, the Jacquard indigo is similar to the S-A and BC indigo samples. The spectrum of Kremer indigo blue lake (10 w% in barium sulfate) (Figure 9), however, is distinct from the three other indigo samples (Table 4). The Kremer pigment's maximum absorption occurs at ~612 nm followed by a more gradual rise to reflectance with an inflection point at ~775 nm; it does not exhibit an absorption at ~860 nm.

These three indigo samples also generally share absorption features in the NIR related to combination and overtone bands positioned at ~1139 nm (3ν CH), ~1670 nm (2ν CH), ~2060 nm (ν+δ NH), ~2160 nm (ν CC + ν CH), ~2280 nm (CC + CH) and ~2408 nm (ν+δ CH) for the

most prominent ones (Tsiantos et al. 2012; Fischer 2020).

The spectrum of the indigo lake (Kremer) exhibits specific absorptions associated to the mordant with bands at ~1450 nm and ~2265 nm, which can be attributed to the -OH first overtone (2ν OH) and combination (ν+δ OH) bands in aluminum hydroxide (Fang et al. 2018), a result consistent with the presence of the mineral gibbsite (Eduardo, Roberto, and Filho 2011). Interestingly, the NIR absorptions of the organic groups NH, CH and CC are quasi absent for the indigo lake, probably because of the interaction with the mordant as similar observations were made when indigo is associated with palygorskite in Maya blue (Tsiantos et al. 2012; Fischer 2020).

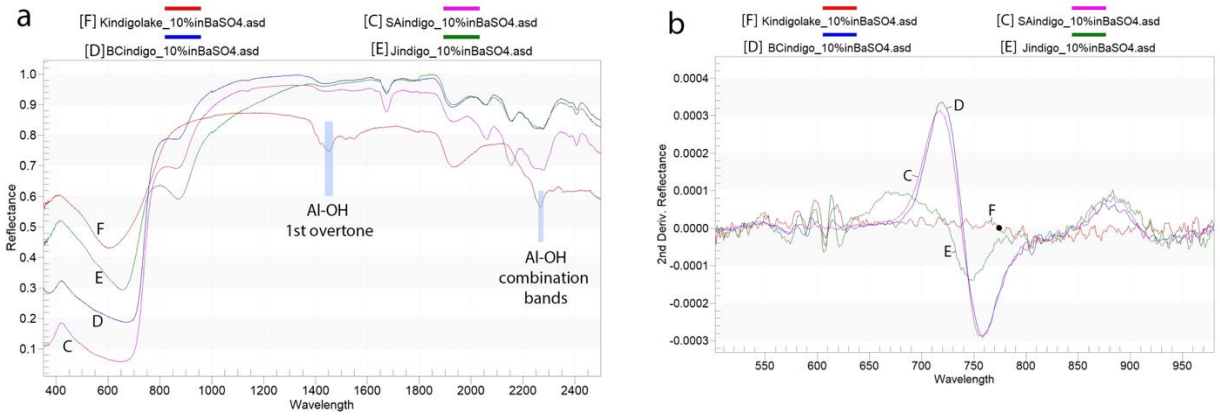

Figure 9. S-A, BC, Kremer, and Jacquard indigo samples reflectance spectra.
a) Mixed (10 w%) with barium sulfate b) Second-order derivative with feature of [F] marked.

Table 4. FORS data for indigo powder reference samples*

Sample & [spectrum]	λ_{ref}max (nm)	λ_{abs}max (nm)	Wavelength of inflection point λ_{inf} (nm)	Secondary absorptions (nm)
S-A 100% [A]	415	~600	745	863, *~1135, ~1540, 1638,* 1675, ~1930, 2060, 2154, 2276, *~2379,* 2407
S-A, 10% in BaSO4 [C]	420	649	738	
BC 100% [B]	419	~600	744	864, *~1135, ~1540, 1638,* 1673, ~1930, 2060, 2155, 2276, *2380,* 2406
BC, 10% in $BaSO_4$ [D]	420	671	740	
Jacquard indigo, 100%	416	~600	736	870, *~1540, 1636,* 1673, ~1920, 2055, 2154, 2273, *~2380,* 2406
Jacquard indigo, 10% in $BaSO_4$ [E]	416	655	726	
Kremer indigo lake, 100%	419	~600	794	*1420,* 1450, *1517, 1546,* ~1935, 2267, *~2313, 2360*
Kremer indigo lake, 10% in $BaSO_4$ [F]	412	612	775	

*For the rest of the tables in the thesis, *italics indicates small absorption,* normal text indicates major absorption, and underlined indicates broad absorption

The results of the FORS analysis of other blue colorants (Table 5) can be categorized into different groups. They will be discussed in order of their similarity to the reflectance spectrum of indigo.

Table 5. FORS data for powder reference samples of blue colorants.
(More information about these samples can be found in Appendix A)

Sample & [spectrum]	λ_{ref}max (nm)	λ_{abs}max (nm)	λ_{inf} (nm)	Secondary absorptions (nm)
Maya blue [G]	430, shoulder at 530	660	764	*~490*, 1417, *1673*, 1918, 2220, *2256*
Smalt [H]	430	544, 595, 643	711	~1200-1800, *2190*
Cobalt cerulean [J]	435	575, 601, 635	701	*~499,* ~1200-1800, *2090*
Cobalt medium [K]	439	551, 585, 624	686	482, ~1200-1500
Lapis lazuli [L]	463	595	714	*~810-825, 1415,* 1917, 2207
Ultramarine [M]	445	598	711	
Egyptian [N]	446	631	691	791, 1045, *1910,* 2218
Han [P]	443	617	680	800, *1910,* 2225
Phthalo [Q]	461	554, 677	856	*~420, 917, 1029,* 1105, 1680, *1720, 1770*, 2150, 2210, 2275, 2350, *2418, 2468*
Heliogen [R]	461	550, 677	856	
Azurite [S]	459	~655	1000	*1405,* 1495, *1888, 1979, 2040, 2213,* 2283, 2351
Prussian, 10% in BaSO4 [T]	440	712	--	1911, *2030, 2090, 2146,* 2372, *2406*

5.1.1.2 Maya blue

As expected, the reflectance spectrum of Maya blue (an organic-inorganic hybrid of indigo and palygorskite clay) (Figure 10a) is very similar to that of indigo in the visible range. Differences are mainly shifts in the peaks: the reflectance maximum of Maya blue in the visible region is red-shifted (to 430 nm) compared to indigo (420 nm) (Leona et al. 2004). This reflectance maximum is followed by a weak absorption at ~490 nm and a shoulder at ~530 nm (absent in indigo samples). Maya blue's main absorption band is narrower (~540-730 nm) than that of indigo (~420-730 nm) (Leona et al. 2004) and there is only a very slight absorption at ~860 nm for Maya blue. The absorptions at ~1417 nm, ~1918 nm, and ~2220 nm are attributed to the clay (palygorskite) component of the pigment; more specifically, these include the -OH

first overtone, H_2O combination bands, and Al-OH combination bands, respectively (Fischer and Kakoulli 2018; Galaxy Scientific 2018).

In the samples analyzed, the first-order derivative (Figure 10) shows that the main absorption of Maya blue is at 660 nm; thus, the wavelength of maximum absorption appears to be roughly the same as the indigo samples. Published literature, however, indicates that the main absorption band of Maya blue shows a red shift to ~660-670 nm compared to that of indigo (660 nm) (Leona et al. 2004); with the current results, this is true if the S-A indigo is considered, but not true for the BC indigo. The first-order derivative clearly shows that the inflection point for Maya blue is red-shifted (to 764 nm) compared to those of the indigo samples.

Leona et al. 2004 explain that a red-shifted absorption band in this case is due to the fact that the HOMO and LUMO energy levels are closer together (Leona et al. 2004). They posit that the spectral differences between indigo and Maya blue in the visible region is a matter of aggregation of indigo molecules due to hydrogen bonding between these molecules versus isolated indigo molecules in the palygorskite lattice in Maya blue (Leona et al. 2004).

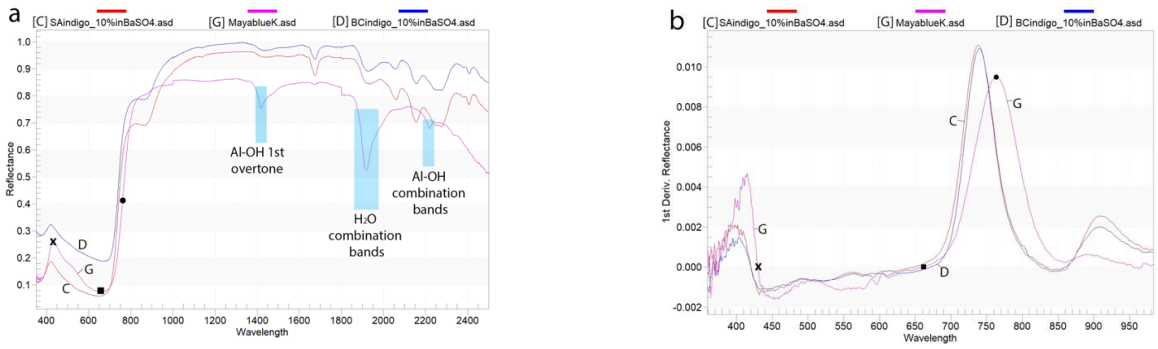

Figure 10. Maya blue reflectance spectrum
a) Compared to indigo samples with feature of [G] marked b) First-order derivative shows that the λ_{abs}max for Maya blue is essentially the same as S-A and BC indigo samples. λ_{inf} for Maya blue is at a longer wavelength (764nm) than for indigo samples.

5.1.1.3 Cobalt pigments

The reflectance spectra of blue colorants containing cobalt (smalt, cobalt cerulean,

cobalt medium) exhibit common features (Figure 11). These three inorganic colorants are produced by heating cobalt salts and making a glassy material that is then ground down into a powder (Kremer Pigmente, n.d.). According to the technical data provided by Kremer Pigments, smalt is a cobalt potassium silicate, cobalt medium is a cobalt aluminate spinel, and cobalt cerulean is cobalt tin oxide (Kremer Pigmente, n.d., 2012, 2018a, n.d., 2018b).

These spectra are characterized by reflectance maxima at ~430-440 nm, absorption bands centered at ~600 nm with triplet features (Fischer and Hsieh 2017); the main absorption band is due to ligand field transitions (Aceto et al. 2014; Fischer and Hsieh 2017). Smalt has absorptions at 544, 595, and 643 nm; cobalt medium has absorptions at ~551, 585, and 624 nm; cobalt cerulean has absorptions at 575, 601, and 635 nm.

The reflectance spectra of these three cobalt-containing pigments exhibit a steep rise to reflection beginning at ~623 nm for cobalt medium, ~643 nm for smalt, and ~618 nm for cobalt cerulean. The inflection points for this transition are at 686 nm for cobalt medium, 701 nm for cobalt cerulean, and 711 nm for smalt. The cobalt pigments exhibit high reflectance in the NIR, which then transitions to another broad absorption beginning at ~1200 nm (Delaney et al. 2005). It is important to note that this transition from absorbance to reflection occurs at wavelengths slightly shorter than this transition for indigo (Figure 11b).

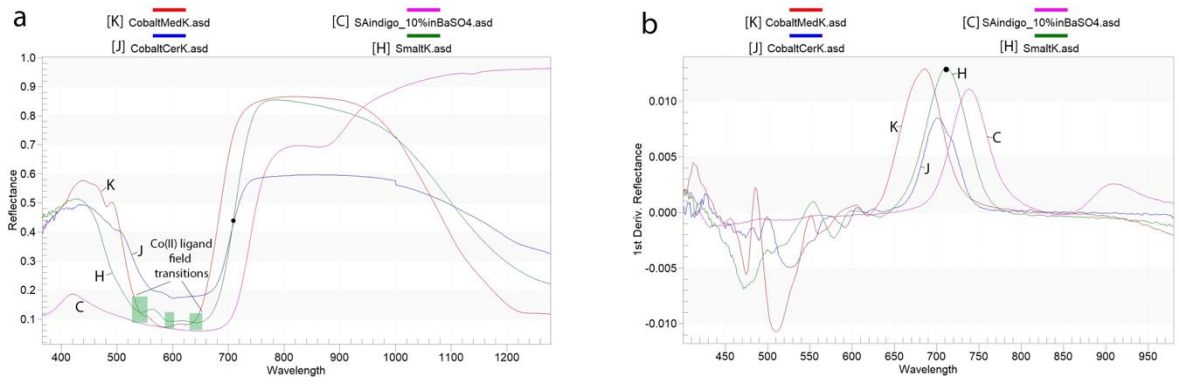

Figure 11. Cobalt pigments reflectance spectra.
a) Compared to indigo with feature of [H] marked b) First-order derivative with features of [H] marked. λ_{abs}max and λ_{inf} for cobalt pigments are shorter than those for indigo.

5.1.1.4 Lapis lazuli and ultramarine

The spectra of lapis lazuli and ultramarine blue (Figure 12) are very similar. Lapis lazuli is a rock that contains the blue mineral lazurite in addition to other silicate minerals (Plesters 1966); the colorant that is obtained by processing the lapis lazuli rock to extract lazurite is called natural ultramarine (Plesters 1966). In the early 19th century, ultramarine blue was artificially synthesized (Plesters 1966). The spectra are characterized by reflection maxima at 445 nm (ultramarine) - 463 nm (lapis), a symmetric absorption band with maximum absorption at 595 nm (lapis) - 598 nm (ultramarine) due to charge transfer transitions (Aceto et al. 2014), inflection points at 711 nm (ultramarine) - 714 nm (lapis), and a weak absorption at ~810-825 nm.

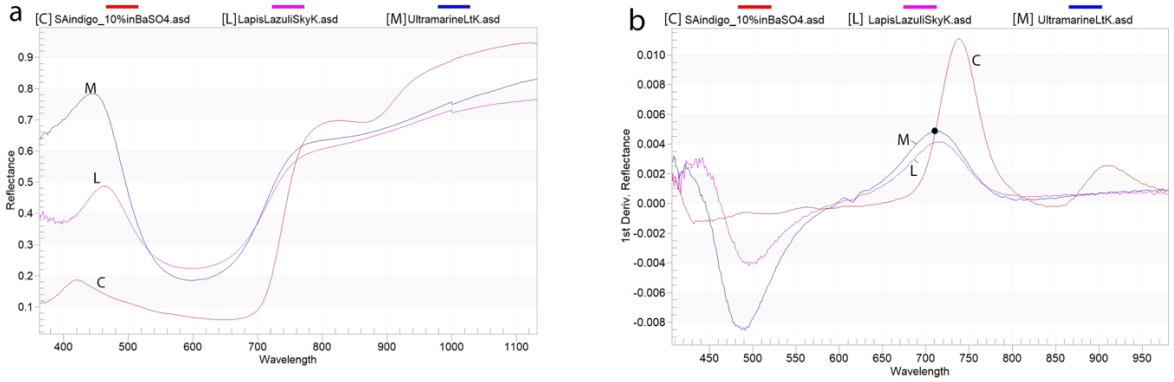

Figure 12. Lapis lazuli and ultramarine reflectance spectra.
a) Compared to indigo with feature of [M] marked b) First-order derivative shows transition from absorption to reflection for ultramarine and lapis lazuli occurs at wavelengths slightly shorter than those for indigo.

5.1.1.5 Egyptian and Han blue

The reflectance profiles of Han blue and Egyptian blue (Figure 13) are similar: they have reflection maxima at ~445 nm, followed by absorption maxima at 617 nm for Han blue and 631 nm for Egyptian blue due to ligand field transitions (Aceto et al. 2014). Both pigments exhibit another absorption band in the NIR (Egyptian at 791nm and Han at 800nm); Egyptian blue exhibits another absorption band at 1045 nm.

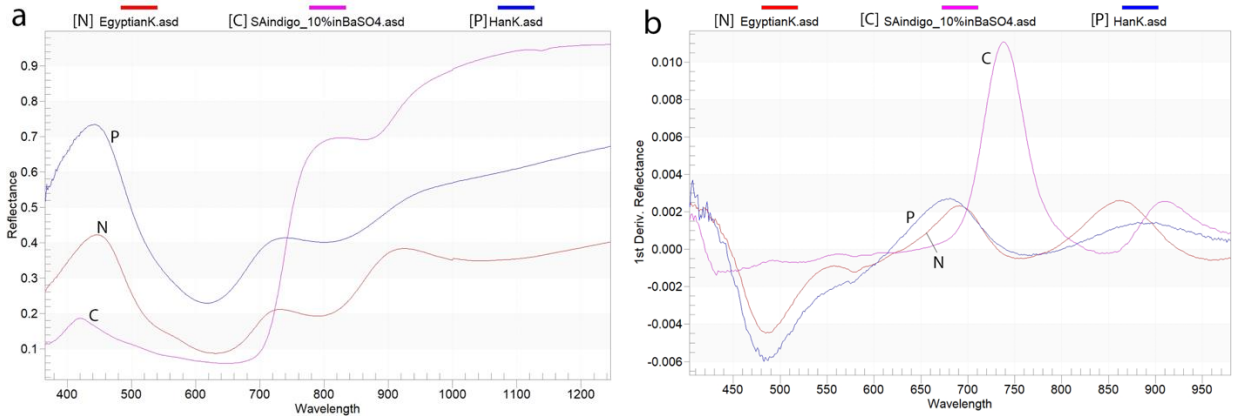

Figure 13. Egyptian and Han blue reflectance spectra.
a) Compared to indigo b) First-order derivative shows that transition from absorption to reflection for Egyptian and Han blues occurs at wavelengths slightly shorter than those for indigo.

5.1.1.6 Phthalo blue

Phthalo blue and Heliogen® blue were discovered to have nearly identical reflectance spectra (Figure 14); this is expected because Heliogen® pigments are a line phthalocyanines manufactured by BASF being sold by Kremer (BASF, n.d.; Kremer Pigmente, n.d.). The reflectance spectra exhibit the following features: reflectance maxima at 461nm, a broad absorption band with a maximum absorptions at ~550 nm and ~677 nm due to ligand field transitions, inflection points at 856 nm, weak absorptions at 917 and 1029 nm, continued rise to reflectance followed by a prominent absorptions at 1105 nm and then a steep rise to maximum reflectance at 1500 nm (Delaney et al. 2005).

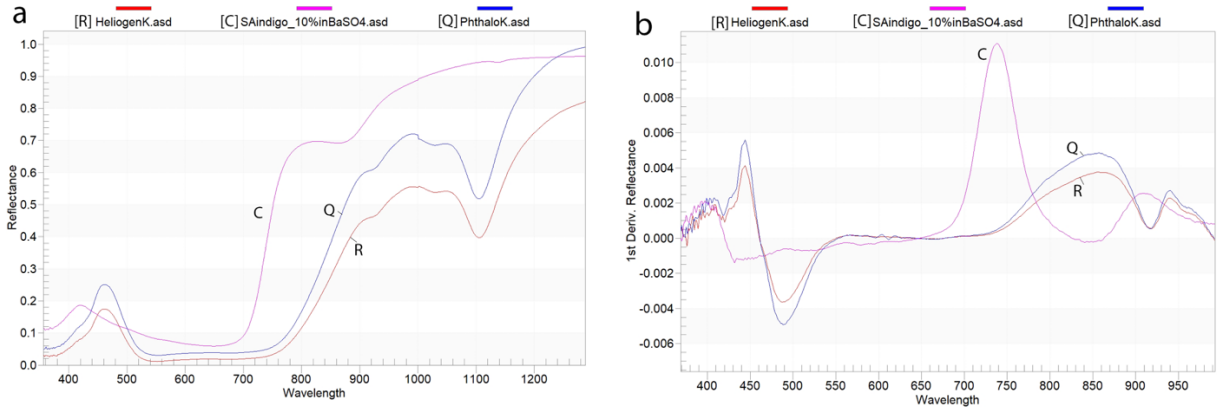

Figure 14. Phthalo and Heliogen® reflectance spectra.
a) Compared to indigo b) First-order derivative shows that transition from absorption to reflection for phthalo and Heliogen® occurs at wavelengths longer than those for indigo.

5.1.1.7 Others

The spectra for azurite and for Prussian blue are outliers (Figure 15). The reflectance spectrum of azurite has a reflectance maximum at 459 nm, followed by a broad absorption with a maximum at 655 nm and a rise to reflectance in the NIR with an inflection point at ~1000 nm (Delaney et al. 2005). The spectrum of Prussian blue exhibits a reflection maximum at 440 nm, followed by a broad absorption with a maximum at 712 nm due to ligand field transitions and a gradual rise to reflection that increases at ~1350 nm (Delaney et al. 2005). Prussian blue was dispersed in barium sulfate (10 w%) because analysis of 100% Prussian blue produced a reflectance spectra with low overall reflectance and poor resolution.

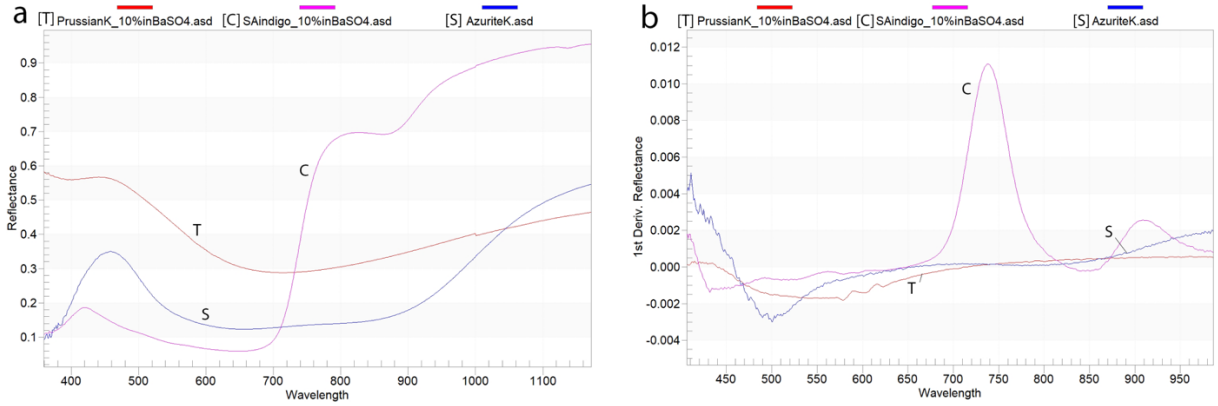

Figure 15. Azurite and Prussian blue reflectance spectra.
a) Compared to indigo b) First-order derivative.

5.1.1.8 Summary

It is no surprise that these blue colorants share reflectance maxima in the blue region (~450 nm) of the visible region of electromagnetic spectrum and maximum absorptions in the yellow to red regions (580-660 nm) (Delaney et al. 2005). Aside from this characteristic, there is quite a bit of variety in the reflectance spectra of the colorants. For the purposes of this study, the regions of most interest are where the maximum absorption and the transition from absorption to reflectance occur. If this transition occurs in the window of the bandpass filters used for the MBRIS (~600-800 nm), this behavior will be expressed in the MBRIS result. In addition to Maya blue, lapis lazuli, ultramarine, and the cobalt-containing pigments have

reflectance profiles that resemble that of indigo in the window in question. FORS results show that these colorants can be distinguished from indigo based upon features outside this window as well as subtle differences inside this window.

5.1.2 MBRIS

Indigo and other blue colorants (Figure 16) were imaged with the MBRIS method. In the MBRIS result, phthalo blue (and Heliogen®), Prussian blue, and azurite appear black. Egyptian blue, Han blue, and Jacquard indigo appear dark grey. S-A and BC indigo, Kremer indigo lake, ultramarine, lapis lazuli, and Maya blue appear lighter grey. Cobalt medium, cobalt cerulean, and smalt appear bright white.

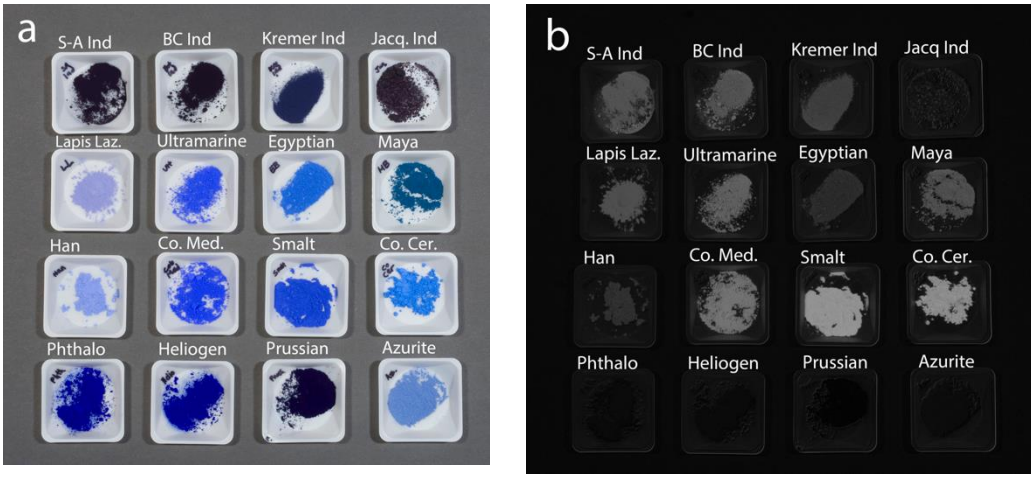

Figure 16. Indigo and other blue colorants powder reference samples.
a) Visible light b) MBRIS result.

The colorants that appear black in the MBRIS are those whose reflectance spectra are dissimilar to that of indigo. More precisely, since MBRIS is based on the subtraction of images taken using two bandpass filters, with transmission at λ_{max} = 660 nm (full width at half maximum (FWHM) = 65 nm) and λ_{max} = 735 nm (FWHM = 90 nm), it is the behavior of the colorants in the red region of the visible and in the NIR that affects their final appearance in the MBRIS result.

The reason that indigo samples (with the exception of Jacquard) appear light using MBRIS method is due to the fact that the λ_{max} = 660 nm BP image captures the colorant near

maximum absorption (Figure 17a). As discussed earlier, the maximum absorption of the indigo powder analyzed with FORS is ~660 nm; the reflectance spectrum does not begin to rise steeply towards reflectance until ~715 nm. The 735 nm BP filter thus captures the colorant near the inflection point of reflectance (Figure 17b). Thus, two bandpass images capture the colorant absorbing and reflecting, respectively. The result of subtracting these images from each other results in a positive difference, which appears as light grey/white in the final image. If the bandpass images capture the colorant behaving the same way in both images (i.e. absorbing at λ = 660 nm and λ = 735 nm), then the subtraction will result in a dark image (black). In other words, the greater the difference in reflectance behavior captured by the two bandpass images, the brighter that area will be in the MBRIS result.

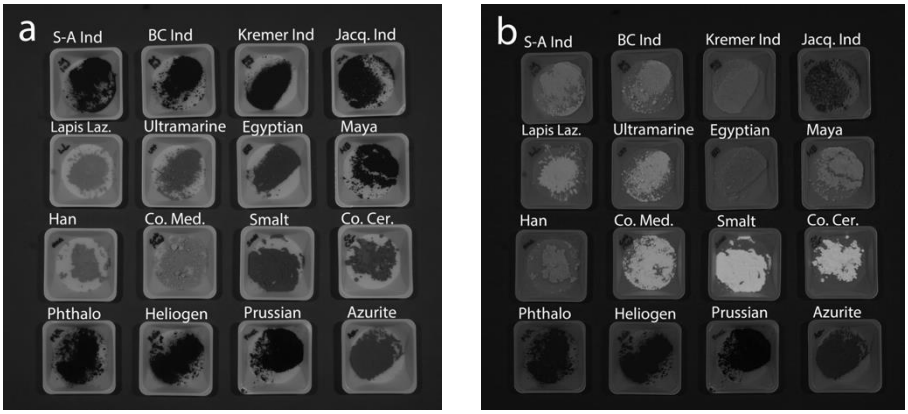

Figure 17. 660 nm and 735 nm bandpass images.
a) 660 nm BP image captures indigo and some of the other colorants near maximum absorption b) 735 nm BP image captures reflectance behavior of indigo and some of the other colorants.

This explains why other colorants with similar reflectance behavior to indigo in the wavelength regions processed by the MBRIS show similar results and create a false positive for indigo identification. The reflectance spectrum for smalt shows that at 660 nm, the pigment absorbs light with λ_{abs}max = 640 nm. In its reflectance spectrum, smalt's inflection point is before 735 nm; therefore, the 735 nm BP filter captures the colorant is strongly reflecting light. Thus, it is no surprise that this pigment appears white using the MBRIS method.

One surprising result is that the Jacquard indigo appears dark in the MBRIS result. In the

735 nm BP image, the Jacquard indigo appears dark, which is not expected given the reflectance spectrum collected from this sample; based on the FORS analysis, this sample should exhibit behavior similar to the other indigo samples at this wavelength. One possible explanation for the unexpected before is that the Jacquard indigo was not in the form of a fine powder (like all the other colorants studied), but rather in larger grains.

5.1.2.1 False-color MBRIS

In the false-color image generated with the MBRIS in the red channel, 735 nm BP image in the green channel, and 660 nm BP image in the blue channel (Figure 18), the samples that contain indigo (with the exception of Jacquard) are the only ones that appear orange. Thus, this false color image provides better data visualization than the MBRIS result alone.

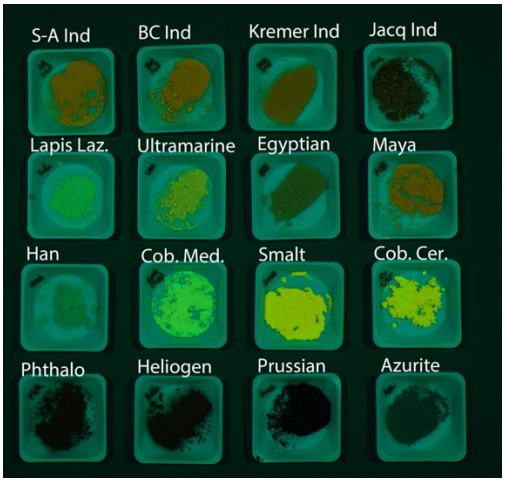

Figure 18. False-color MBRIS.
Indigo-containing colorants appear orange.

5.1.2.2 Effects of concentration

In order to explore how the concentration of indigo affects the MBRIS results, different amounts of indigo powder were mixed with barium sulfate (Figure 19a) and imaged using the MBRIS method (Figure 19b). The concentrations tested include: 0.5, 1, and 10 w% in barium sulfate. 0.5% was selected as the lowest concentration due to the sensitivity limitations of the balance. For the 0.5% concentration, the powder barely appears lighter than the background in the MBRIS result. This may indicate a qualitative limit of detection. The 1 w% indigo in barium

sulfate mixture appears distinctly brighter than the background in the MBRIS result.

This suggests that, for trace amounts of indigo or degraded surfaces, the MBRIS method may not clearly indicate indigo's presence, thus creating a false negative result. It is also noteworthy that, although the two indigo colorants tested produce similar results, the synthetic S-A indigo appears to have greater tinting strength than the BC indigo. This is evident in the 1 w% and 10 w% concentrations both in visible light and in the MBRIS result image. In the visible light image, the S-A indigo mixtures appear deeper blue than the BC indigo mixture; in the MBRIS result, the S-A mixtures appear slightly brighter than the BC mixtures.

Useful further studies would include similar concentration tests with the other blue colorants that produce MBRIS results similar to indigo, such as those that contain cobalt and lapis lazuli.

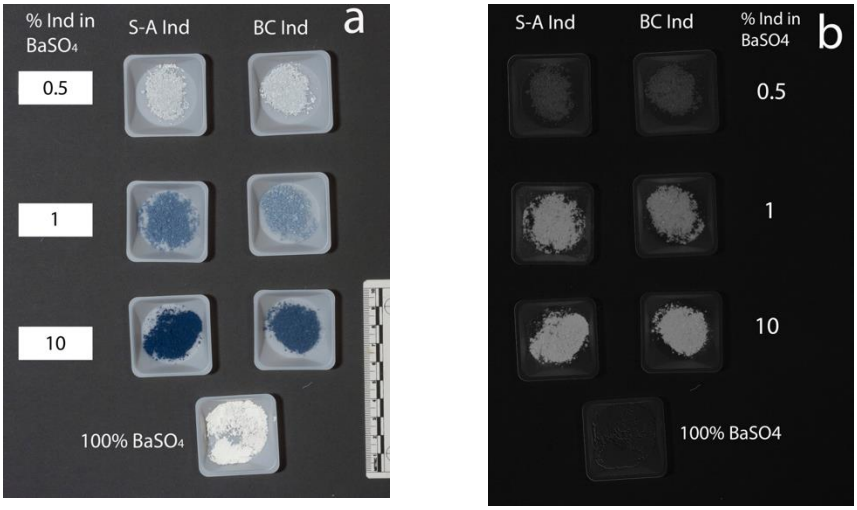

Figure 19. Different mixtures of indigo and barium sulfate.
a) Visible light b) MBRIS result

5.1.3 HSI

The processing of the spectral images at narrow bandwidths to build a false-color image provides a robust method that not only identifies indigo, but also can differentiate it from other blue colorants with similar reflectance behavior in the visible and NIR. Using the Specim IQ hyperspectral camera and the proprietary software Specim IQ Studio, it is possible to select the

wavelengths in order to build a false-color trichromatic image using the RGB channels; the presets on the channels are set for calibrated RGB at R = 598 nm, G = 548 nm, and B = 449 nm. This means that what appears red in the image uses a band at 598 nm, what appears green uses a band at 449 nm, and what appears blue uses a band at 449 nm. If the red channel is changed to 800 nm, for example, materials that reflect NIR radiation at 800 nm will appear red. The overall reflection is given by the y-axis of the reflectance spectrum. For each pixel (and each spectrum), the program identifies the position of maximum reflectance is and assigns a color to that wavelength based upon the location of the RGB channels.

By selecting in the red channel (R) in the small absorption of indigo at 862 nm, in the green channel (G) the inflection point at 740 nm, and in the blue channel (B), the main absorption at 660 nm, the resulting false-color images show a good distinction amongst the various blue pigments (Figure 20a). The differentiation between indigo and Maya blue still remains challenging owing to their similar spectra and would require additional processing.

The resulting false-color image shows that the indigo samples (with the exception of Jacquard) and Maya blue appear orange. This is because the highest overall reflectance for indigo occurs in the orange region within the range of the defined RGB channels (660-860 nm). For the cobalt containing pigments, the highest reflectance occurs in the yellow region. The false color image provides greater differentiation of the colorants than the MBRIS result. In a similar fashion, differentiation can be achieved by manipulating the RGB channels so that R = 860 nm, G = 740 nm, and B = 420 nm, the maximum reflectance in the visible for indigo (Figure 20b).

Figure 20. Powder reference samples HSI.
a) Screenshot of Specim IQ Studio software with false-color image generated with RGB channels set to 862, 738, and 660 nm, respectively. The wavelengths correspond to the wavelengths of small absorption, inflection point, and maximum absorption of indigo, respectively. Spectrum shown from S-A indigo. b) RGB channels set to 860, 740, and 420 nm, respectively. The wavelengths correspond to the wavelengths of small absorption, inflection point, and maximum reflectance of indigo in the visible region, respectively.

5.1.3.1 Effects of concentration

For the concentration tests, the Specim IQ Studio software was used to generate a false-color image (Figure 21a) with RGB channels set to 860, 740, and 660 nm, respectively. The resulting image (Figure 21b) shows the 10 w% mixture with a dark orange color, the 1 w% orange-yellow and the 0.5 w% pale yellow. The pure barium sulfate is almost perfectly reflecting across the entire spectral range and thus appears white (Figure 21c). With increasing quantity of indigo added into barium sulfate, the magnitude of the difference between the maxima in absorption and reflectance increases and affects the shape of the reflectance profile. For the 0.5 w% mixtures (Figure 21d), the maximum reflection occurs in the yellow range because the transition from absorption to reflectance is small in magnitude and the inflection point occurs well before 740 nm. With increasing concentration of indigo, the transition from absorption to reflection is larger in magnitude and the inflection point becomes further red-shifted (Figure 21e-f). Thus, with increasing concentration of indigo, the maximum reflectance occurs closer to the red region of the defined RGB range.

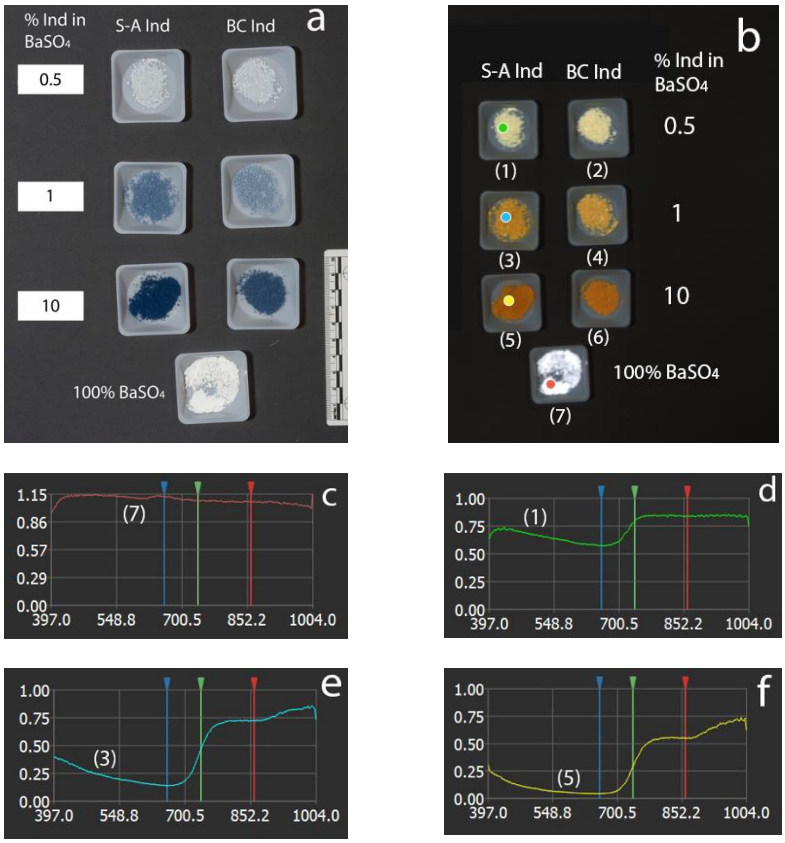

Figure 21. HSI on concentration tests.
a) Visible light b) False-color hyperspectral image of different concentrations of indigo samples in barium sulfate. RGB channels set to 863, 740, 660 nm respectively c) Spectrum from 100% barium sulfate d) Spectrum of 0.5% S-A indigo in barium sulfate e) Spectrum of 1% SA indigo in barium sulfate f) spectrum of 10% S-A indigo in barium sulfate.

5.2 Paint swatches

After preparing the paint swatches (

Figure 22a) on the dark background, it became apparent that many of the colorants were applied too thinly and thus the dark background was highly visible through the blue layer. The need to more carefully standardize amount of pigment added to the medium as well as the thickness of the applied paint became apparent.

5.2.1 FORS & MBRIS

As suspected, many of the samples produced spectra with low overall reflectance that were difficult to interpret. This is likely due to the contribution of the dark background. If

repeated, paint swatches would be done on a lighter background in order to mitigate the problem of low overall reflectance. For discussion of FORS results see Appendix B.

The MBRIS method on the paint swatches (Figure 22b) provided the following results: the whitest results were given by S-A indigo and cobalt cerulean; BC indigo and Jacquard indigo appeared light grey; Maya blue, Kremer indigo, lapis lazuli, smalt, ultramarine and cobalt medium appeared darker grey. However, as mentioned above, before drawing conclusions, it would be important to redo this setup being sure to standardize the ratio of dry pigment to medium, and the amount of paint applied in the swatch.

Despite this experimental error, one interesting result is that the MBRIS seems to provide an indication of the thickness of the paint film applied, which is harder to observe in visible light due. In the false-color MBRIS result (Figure 22c), the cobalt cerulean swatch appears orange; interestingly, the colorant appears yellow in powder form (Figure 18). This may indicate that the false-color MBRIS method may not be a reliable tool for differentiating the blue colorants, especially when mixed with a binder. Because the experimental setup was flawed, no further results will be discussed.

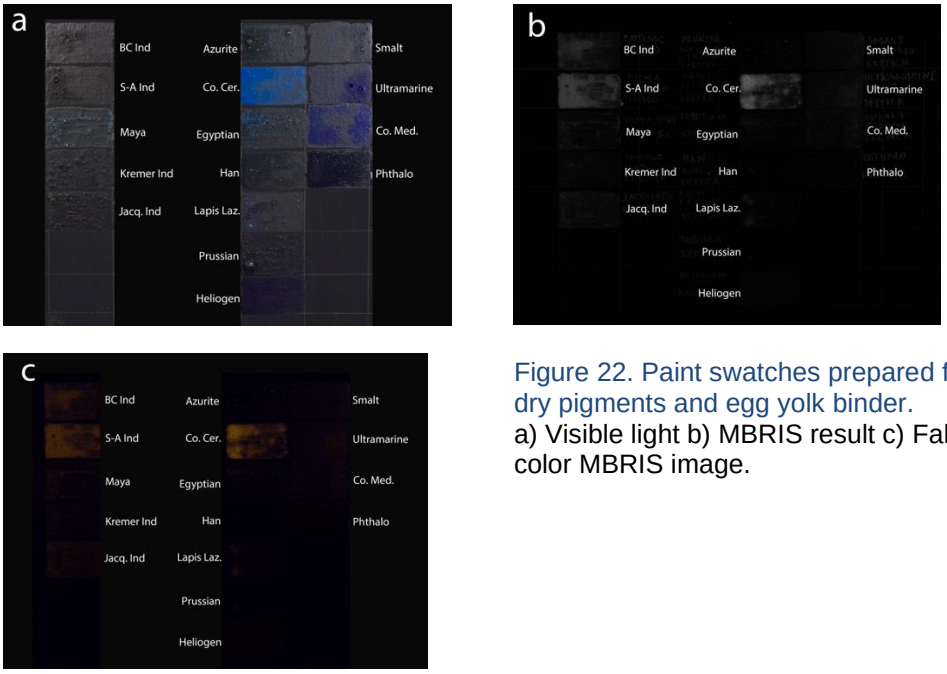

Figure 22. Paint swatches prepared from dry pigments and egg yolk binder.
a) Visible light b) MBRIS result c) False-color MBRIS image.

5.3 Indigo dyed fiber substrates reference samples

Different fiber substrates were dyed with two types of indigo for varying amounts of time to compare the results of colorant concentration, substrates, and indigo source.

5.3.1 FORS

FORS on the indigo-dyed fiber substrates produced reflectance spectra that shared the same characteristic absorptions as those measured on powdered indigo samples, namely a main absorption at ~660 nm, and secondary absorption at 860 nm (Table 6).

When spectra of the dyed fabrics are compared to the spectra of the indigo powder (10 w% in barium sulfate), there are differences worth noting. The dyed fabric samples exhibit broader, red-shifted reflection peaks in the visible region compared to the powdered samples (Table 6); generally, shorter dye times correspond to greater red shifts for this peak. With this effect on the reflection peak, the main absorption band becomes narrower.

A trend common to all dyed samples is that the inflection points are blue-shifted for the dyed fabrics compared to the powdered dye (Table 6, Figure 23). Generally speaking, for the samples analyzed, the magnitude of this blueshift is greater for the samples with shorter dye times. This blueshift occurs with all fabrics tested and is not specific to proteinaceous or cellulosic fibers.

The extent to which the small absorption at 860 nm is apparent in the reflectance spectra appears to be related to the dye time and thus the amount of indigo present. In general, this absorption is more likely to be present in the samples with the longer dye times. For example, for the cotton and wool dyed with S-A the absorption is clearly present in the longest dye time, less pronounced for the single and double 5 min dye times, and even less apparent in the single and double 2 min dye times. The BC dyed cotton and wool samples do not show this absorption as well; even in the spectrum from the longest dye time, this absorption is only slightly apparent.

Silk samples (S-A and BC dyed) (Table 7) are unique in that the wavelength of the main absorption spans a broader range than the other fabrics; in general the main absorptions for the shorter dye times are blue-shifted as far as 623 nm for the S-A silk dyed for 30 s (Figure 24).

When the wavelengths of maximum absorption for dyed fabrics were compared to the powdered indigo, the trend seems to depend on the source of indigo. With the cotton dyed with S-A, there is a slight red-shift in the wavelength of maximum absorption compared to the powdered samples; 10% S-A indigo in barium sulfate had a maximum absorption at 649nm while the S-A dyed fabric samples (wool, cotton, llama) had maximum absorptions 653-660nm. There was no clear trend with S-A dyed silk. However, for fabrics dyed with BC indigo, their maximum absorptions were slightly blue-shifted compared to the powdered indigo. For a mixture of 10% BC indigo in barium sulfate, the maximum absorption is at 671 nm, while on cotton, wool, and llama, it is located between 654 nm and 659 nm; as noted above, the maximum absorptions for the BC dyed silk ranged from ~628-650 nm.

More analysis needs to be done in order to find a definitive attribution for the blue and red shifts observed; generally speaking, these shifts exhibit trends that correspond to the amount of dye time, and thus likely the amount of indigo present. A place to start with further research would be to compare FORS spectra of undyed fiber substrates to those dyed for various amounts of time. It is likely that the shifts observed in the FORS spectra arise from the reflectance profiles of the base materials (i.e. fiber substrates) in the visible region.

Table 6. FORS data on selected dyed fiber substrate samples.

	λ_{ref}max (nm)		λ_{inf} (nm)	
Dye Time	**S-A dyed cotton**	**BC dyed wool**	**S-A dyed cotton**	**BC dyed wool**
10 min, 20 min	423	434	726	722
5 min x 2	428	431	717	724
2 min x 2	440	453	710	717
30 s	499	503	698	701

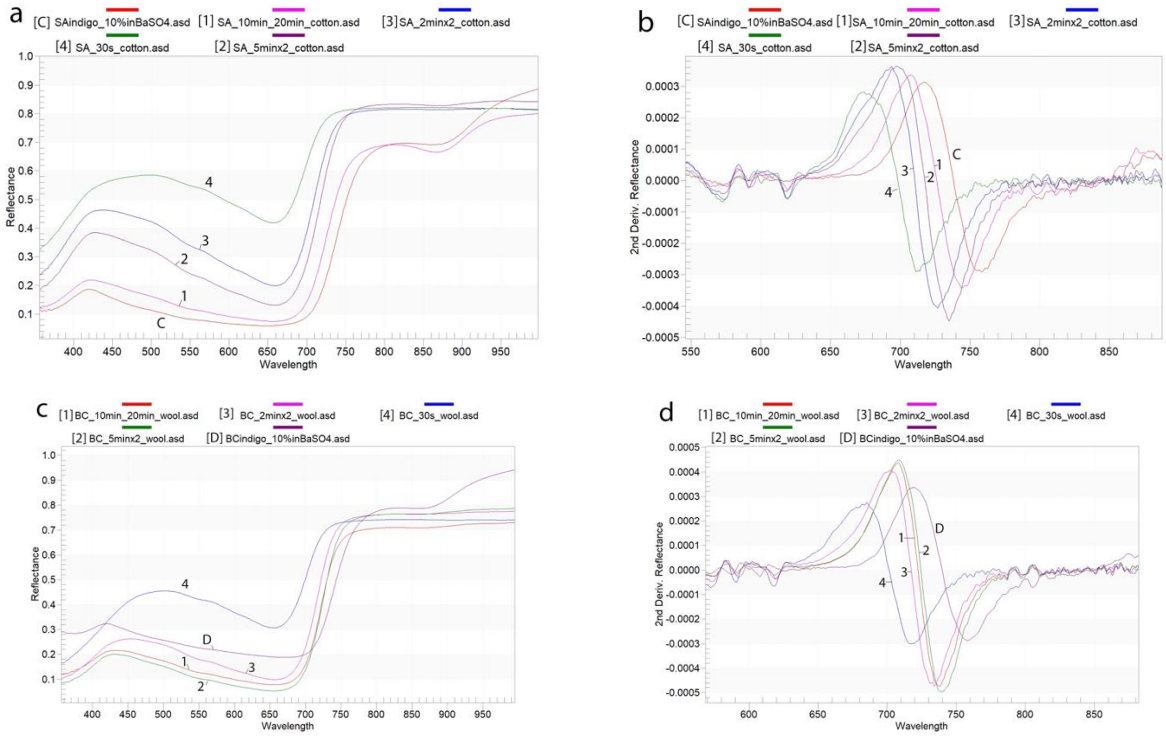

Figure 23. S-A dyed cotton and BC dyed wool.
a) S-A dyed cotton reflectance spectra show that $\lambda_{ref}max$ broadens and shifts to longer wavelengths with decreasing dye time b) Second derivative shows that λ_{inf} are blue-shifted for dyed samples, with shorter dye time corresponding to greater blueshift c) BC dyed wool reflectance spectra show similar trend to S-A dyed cotton d) Second derivative shows that λ_{inf} are blue-shifted for dyed samples, with shorter dye time corresponding to greater blueshift.

Table 7. Comparison of $\lambda_{abs}max$ on silk versus other fiber substrates.

	λ_{abs}max (nm)					
	30 s	**2 min x 1**	**2 min X 2**	**5 min X 1**	**5 min X 2**	**10 min, 20 min**
S-A dyed silk	623	626	650	625	657	650
BC dyed silk	628	632	641	654	654	653
S-A dyed cotton, wool, llama	653-660					
BC dyed cotton, wool, llama	654-659					

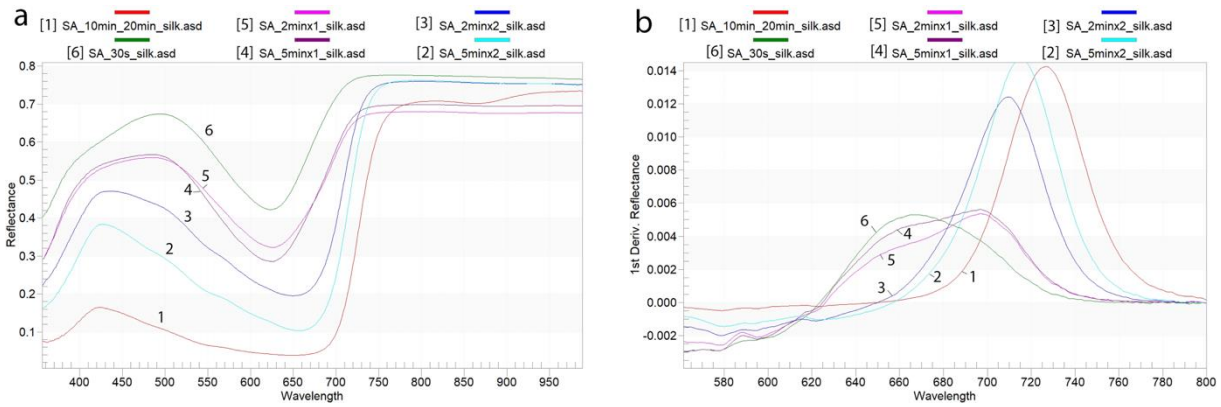

Figure 24. S-A dyed silk.
a) Reflectance spectra. Amount of dye time affects location of main absorption b) First derivative shows the range of main absorptions (where 1st derivative passes through zero) for silk dyed with S-A indigo.

5.3.2 MBRIS

The MBRIS method provided results consistent with what is observed in the visible light image (Figure 25a). All dyed samples appear brighter than the background and the undyed samples in the MBRIS result (Figure 25b). Even the samples dyed for the shortest amount of time appear brighter than the background and undyed samples in the MBRIS result. This indicates that MBRIS technique is sensitive to this low concentration of dye.

Generally, samples that appear lighter blue in visible light appear darker in the MBRIS result; this is likely due to the fact that there is less indigo on these samples. Spots on which less dye was deposited during dyeing appear as darker areas in the MBRIS result.

The fabric substrate appears to play an important role in what is imaged with the MBRIS method. The dyed sample that appears the deepest blue is the S-A wool sample dyed for 30 minutes total; it clearly stands out in the visible image as the darkest. However, this is not reflected in the MBRIS result. Instead, the two cotton samples dyed for 30 min appear brighter white in the MBRIS result. This discrepancy is likely due to the fact that, compared to the wool, the cotton has a denser weave and is composed of thicker threads, which makes it appear less transparent and opaquer. The opacity and thickness of the fabric substrate, in addition to concentration of dye, appears to affect the MBRIS result.

To expand on this work, it would be beneficial to include different dyes for comparison with indigo and to explore mixtures of indigo with other dyes.

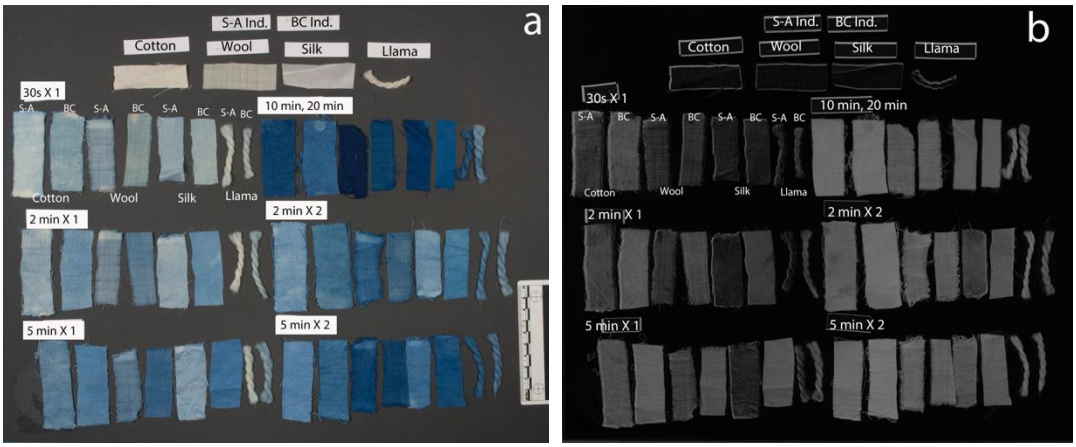

Figure 25. Dyed fiber substrate reference samples.
a) Visible light b) MBRIS result.

5.3.3 HSI

Using the Specim IQ Studio software, a false-color image was generated by changing the RGB channels to 860, 740, and 660 nm, respectively. In this false-color image (Figure 26b), most of the samples appear yellow-green. In the false-color images generated for the powdered samples (Figure 20), indigo appears orange. This shift is consistent with the observations made in the FORS analysis of the dyed fiber substrates: compared to powdered indigo, fiber substrates dyed with indigo exhibit blue-shifted inflection points. Thus, in this hyperspectral image, the maximum reflectances of the samples (Figure 26d) occur closer to the defined green wavelength (740 nm) than they do in the false color hyperspectral images of indigo powder samples.

Several of the silk samples (Figure 26c) appear bluer in the false-color image; the blue-shifted spectral features observed in the FORS data (Table 7) likely accounts for this difference in appearance in the false-color image.

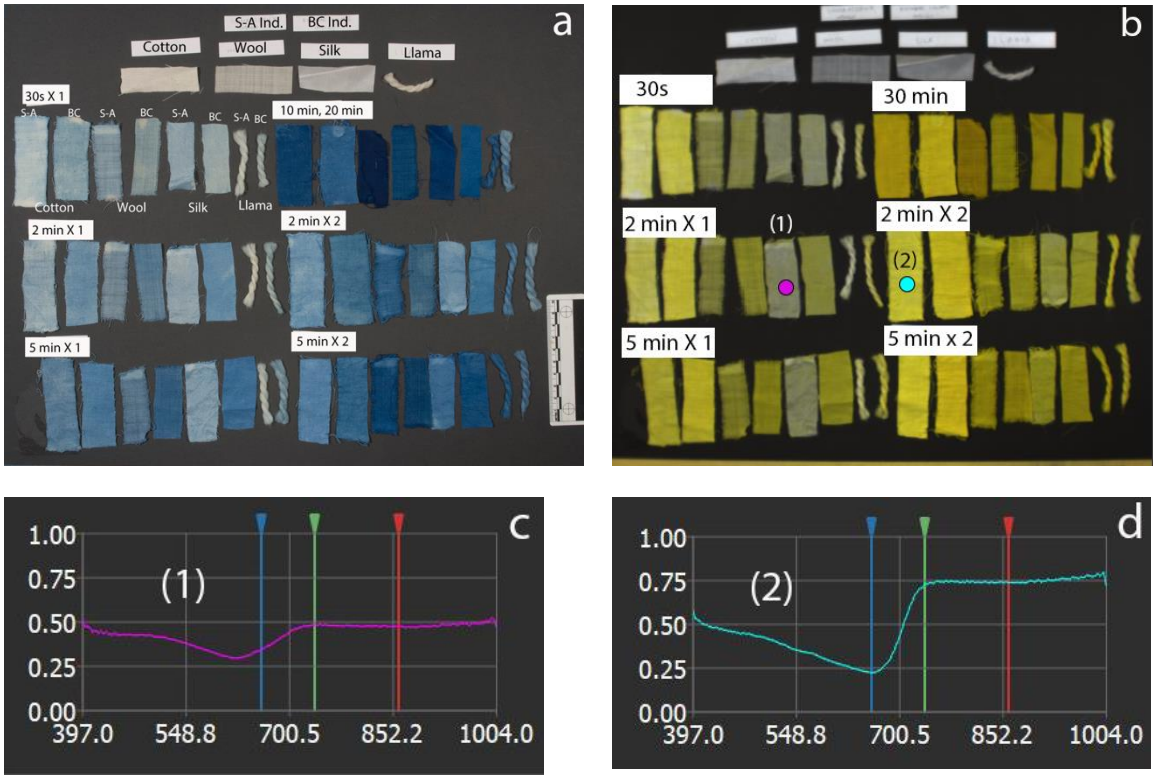

Figure 26. Dyed fiber substrate samples.
a) Visible light b) False-color hyperspectral image of dyed fabrics with RGB channels set to 863, 740, 660 nm respectively c) Spectrum of S-A silk, 2 min d) Spectrum of S-A cotton, 2 min X 2.

5.4 Archaeological and ethnographic objects

Several objects from the Fowler Museum were analyzed using FORS, the MBRIS method, and HSI. These objects include textiles from South America and Africa, ceramics from Central America, and paintings from Indonesia.

5.4.1 Peruvian textile fragment (X2011.31.34)

5.4.1.1 FORS

On this textile fragment (Figure 27a), FORS measurements (Figure 27b) were taken from the undyed fabric and all areas with colored yarns with particular emphasis on the central green yarns believed to have been dyed with indigo.

Figure 27. Peruvian textile fragment (X2011.31.34)
a) Obverse b) FORS measurement locations. Note two smaller spots labeled in central panel.

FORS analysis (Table 8) on this object was limited by the fact that the spot size of the instrument is about 8mm, which is larger than areas of single colors on the figural panels, including the light green believed to be indigo. Spots were selected to minimize input from other colors. Even with contributions from other colors in the spectra, the results were informative.

The measurement taken on the red area [0] of the object shows a reflectance spectrum that is distinct from the spectra collected from the green [1] and tan [2] areas (Figure 28a); the red area has a main absorption around ~520 nm, then rises to reflectance with an inflection point at ~605 nm. The green and tan areas produce reflectance spectra with maximum absorptions at ~605-625 nm, and inflection points at ~710 nm. The similarity of the spectra collected from the green and tan areas may indicate that the tan areas are undyed and the green areas contain some dye but in a low concentration.

To reduce the instrument's spot size, the FORS probe was removed from the instrument head; the probe and light source were held by hand at a 45° angle from each other. This modification helped to better resolve the green area from the dark purple background adjacent to it. This second round of measurements (Figure 28b-c) made clear that the green area produced a reflectance spectrum distinct from the adjacent purple color. The reflectance spectrum from the green area [P0] has a maximum absorption at 652 nm, steep rise to reflection, and an inflection point at 716 nm. These features are consistent with indigo; the blue-

shifted inflection point is also consistent with the results given by reference fabrics dyed with indigo discussed in the section 5.3. The spectrum from the dark purple area [P1] does not exhibit these features and thus is it less likely that it contains indigo.

When spectra from the object were compared to spectra taken from the dyed fiber reference samples (Figure 28d), features in the NIR indicate that the substrate is potentially wool or camelid fiber; spectra from the textile exhibit an absorption at ~1750 nm, which is shared by the wool and camelid reference samples (Galaxy Scientific 2018).

Table 8. X2011.31.34 FORS data.

Sample name & [spectrum]	**Description**	**λ_{ref}max (nm)**	**λ_{abs}max (nm)**	**λ_{inf} (nm)**
X2011_31_34_0 [0]	red	--	~520	605
X2011_31_34_1 [1]	green + purple	--	~605	714
X2011_31_34_2 [2]	tan	--	~624	709
X2011_31_34_probe_0 [P0]	green	~526	652	716
X2011_31_34_probe_1 [P1]	purple	~462	~559	--

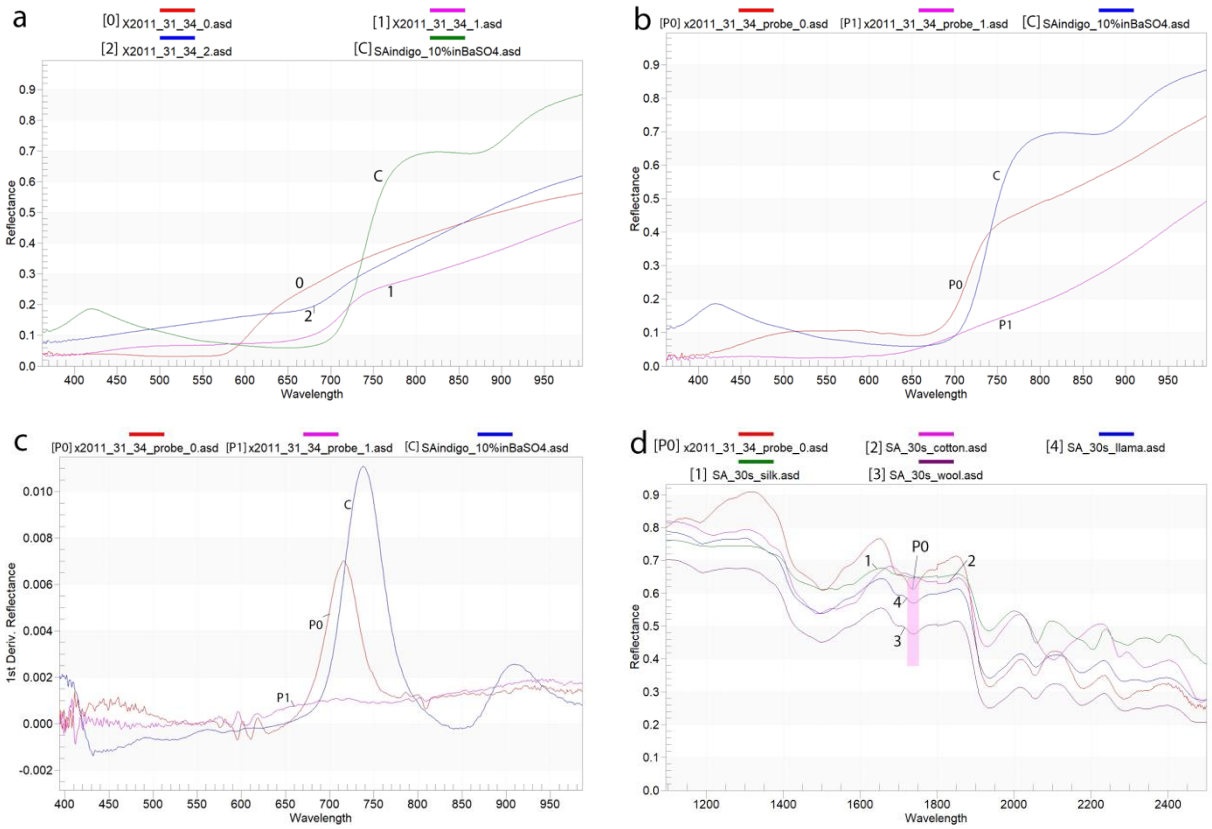

Figure 28. FORS spectra collected on the Peruvian textile (X2011.31.34)
a) Spectra show that [0] has different absorption in visible b) Smaller spot size provides clear distinction between dark purple [P1] and green [P0] areas c) First-order derivative shows that [P0] shares similar λ_{abs}max and λ_{inf} with indigo d) Reflectance spectra compared to those of reference fabric samples. Absorptions at ~1740 nm and ~2175 nm suggest that X2001.31.34 contains wool or camelid fiber as opposed to cotton or silk.

5.4.1.2 MBRIS

In the MBRIS results (Figure 29), the green threads appear white and much brighter than the rest of the textile. These data may suggest the presence of indigo, though blue pigments other than indigo have also shown similar outcomes using this method.

This is an example where MBRIS can supplement FORS; because the spot size of the FORS instrument was larger than the features being analyzed, the MBRIS result complement the spectral information by providing a map of the entire object.

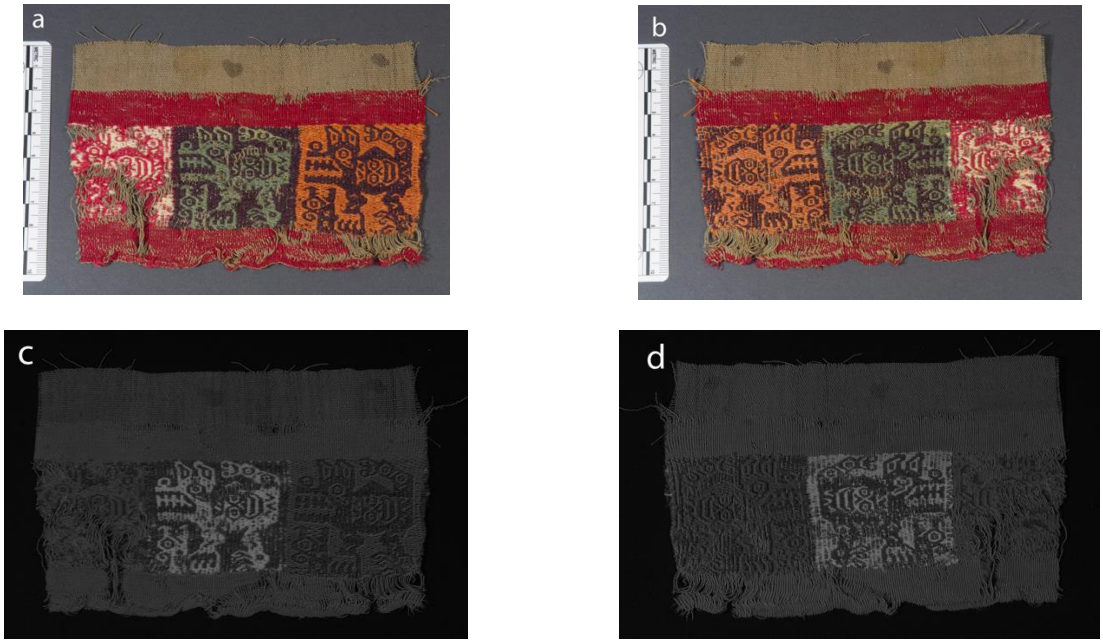

Figure 29. MBRIS results for X2011.31.34.
a) Obverse, visible light b) Reverse, visible light c) Obverse, MBRIS result d) Reverse, MBRIS result. In c) and d) area with green threads appears brighter than the rest of the object.

5.4.1.3 HSI

In the false-color image generated by the Specim IQ Studio software (Figure 30), the green areas appear golden when the RGB channels are set to 860, 740, and 660 nm respectively. The fact that these areas appear golden, not orange as with the powdered indigo, is consistent with the blue-shifted inflection points found in the dyed fabric samples.

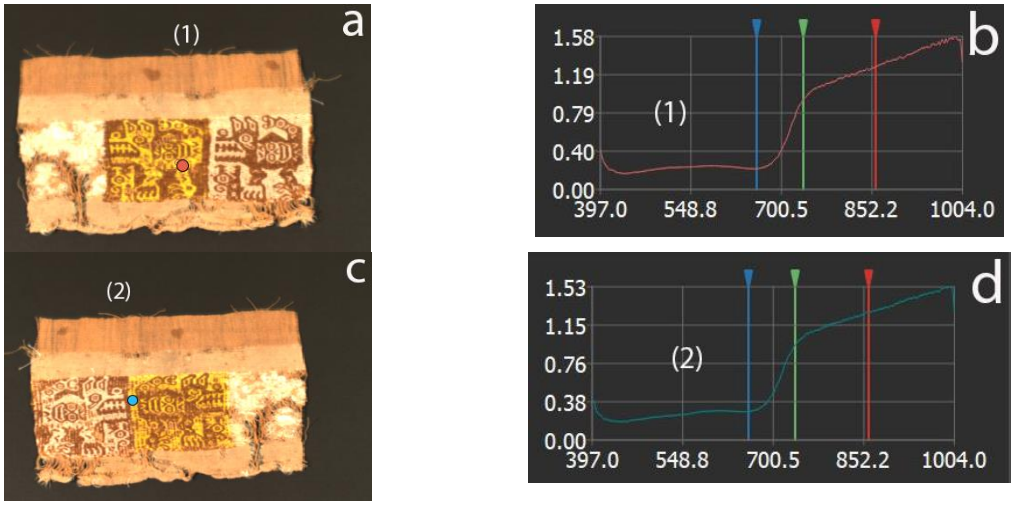

Figure 30. HSI on X2011.31.34.
a) False-color hyperspectral image with RGB channels set to 862, 740 and 660 nm respectively b) Spectrum from area dyed with indigo c) False-color hyperspectral image of reverse with RGB channels set to 862, 740 and 660 nm respectively d) Spectrum from area dyed with indigo.

5.4.2 Skein from Mali (X90-271)

5.4.2.1 FORS

FORS analysis was performed on several spots of this skein of cotton yarn (Figure 31) partially dyed with indigo. Measurement spots (Figure 31b) were selected to include the range of colors visible on the object.

The reflectance spectrum from an area free from dye to the naked eye [1] shows a high overall reflectance and only the slightest absorption at ~637 nm (Figure 32a). Spectra from light [2] and medium [3] blue areas exhibit maximum absorptions at 646 nm and 639 nm respectively. The inflection point for the light blue area is at 710 nm and for the medium blue area at 730 nm. The spectra from areas that appear deep blue [4-5] show broad absorptions in the visible with rise to reflectance beginning at ~660 nm and inflection points at ~735 nm. These spectra also showed the absorption at ~860 nm that is observed in the pure indigo powders as well as the reference dyed fabrics immersed in the vat for the longer durations. Thus, this absorption is likely linked to the concentration of the dye present.

The results from X90-271 (Table 9) are consistent with other findings in this study. Namely, that the small absorption at ~860 nm is connected to concentration of indigo and that lighter color (lower dye concentration) on a dyed sample is associated with a blue-shifted inflection point (Figure 32b-c). The absorptions at ~1780 nm and ~2100 nm are consistent with the cotton reference samples (Figure 32d).

Table 9. X90-271 FORS data.

Sample name & [spectrum]	Description	λ_{ref}max (nm)	λ_{abs}max (nm)	λ_{inf} (nm)	Absorption at ~860 nm?
X90_271_1 [1]	Undyed	--	*637*	705	no
X90_271_2 [2]	Light blue	567	646	709	no
X90_271_3 [3]	Medium blue	--	639	730	yes
X90_271_4 [4]	Deep blue	--	Broad abs	735	yes
X90_271_5 [5]	Deep blue	--	Broad abs	734	yes

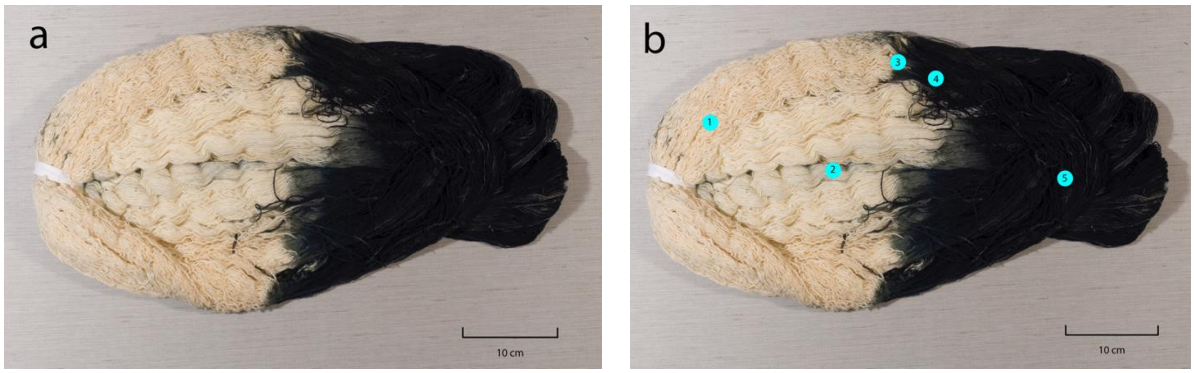

Figure 31. Skein from Mali (X90-271)
a) Visible light b) FORS measurement locations.

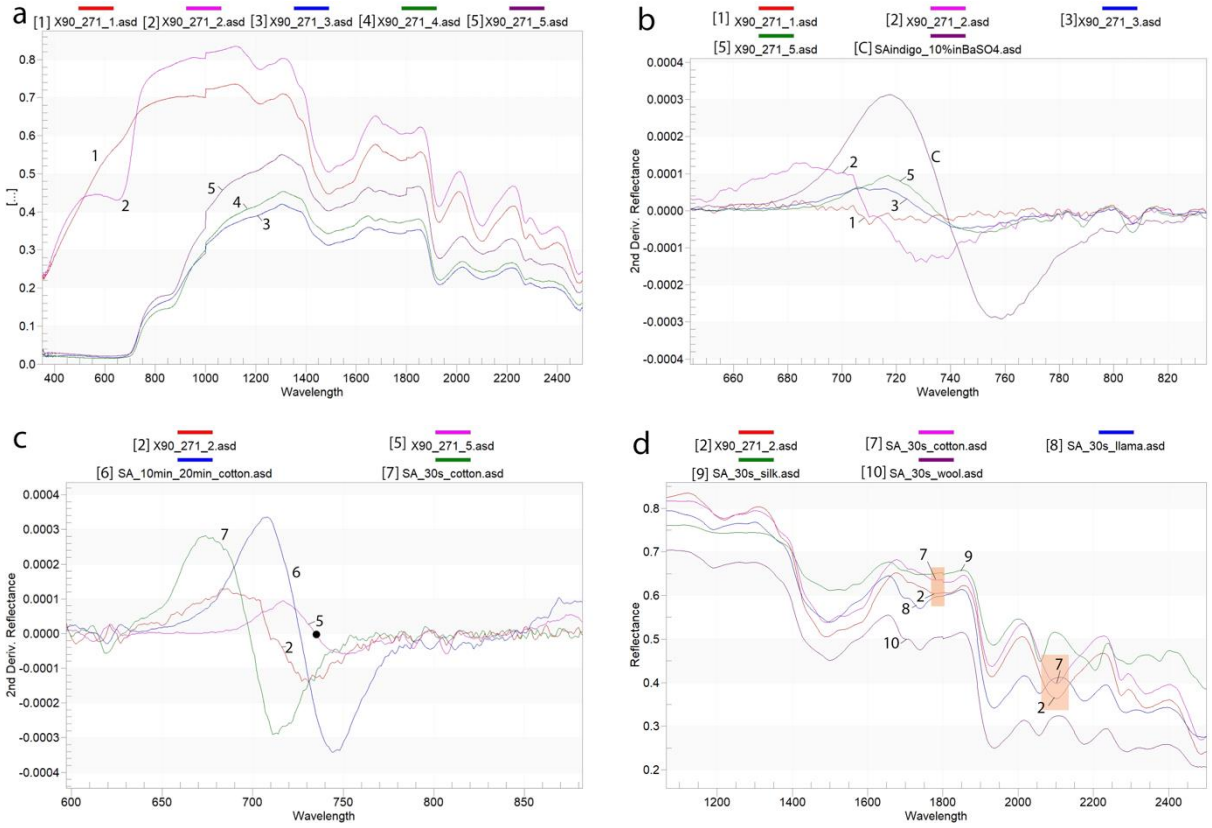

Figure 32. X90-271 reflectance spectra.
a) Absorption at ~860 nm is present in areas with higher indigo concentration b) Second derivative shows that λ_{inf} are blue-shifted corresponding to lower indigo concentration c) Second derivative shows trend of blue-shifted λ_{inf} for lower indigo concentration on reference samples and on X90-271 d) X90-271 and cotton reference are the only spectra that exhibit absorptions at ~1780 nm and ~2100 nm.

5.4.2.2 MBRIS & HSI

The MBRIS image (Figure 33b) for X90-271 produced unexpected results. It was

expected that the side of the skein that appears saturated with dye would appear bright white in the MBRIS result. However, this is not the case. In fact, the deep blue side of the object appears darker overall than the undyed side in the MBRIS result. The areas of the image that appear brightest correspond to areas that apparently contain a low or intermediate amount of colorant.

The FORS analysis of X90-271 provides an explanation for the MBRIS result. The spectra from the deep blue area [4-5] have low overall reflectance, likely due to the high concentration of the dye. Spectra from areas where only a low or intermediate amount of dye is present [2-3] produce spectra with higher overall reflectance. In the spectra, the magnitude of the transition from maximum absorption to reflectance beginning at 660 nm is significantly greater for [2] than for [5]. The MBRIS method used here captures that transition; thus, these results indicate that it appears that where this transition is greater in magnitude, a brighter result will be produced with the MBRIS method.

In the false-color hyperspectral image (Figure 33c) with the RGB channels set to 860, 740, and 660 nm respectively, the areas that appear golden (as observed in the false-color image of X2011.31.34) are those that appear to have little to intermediate amounts of colorant. Examination of the spectra (Figure 33d-e) from the hyperspectral image indicates what was found with the FORS analysis: that the magnitude of the transition from absorption to reflectance is greater in magnitude for areas with little to intermediate amounts of colorant.

This example illustrates that high concentrations of indigo could be problematic with the MBRIS method. In other words, the MBRIS method may not produce an accurate map of indigo in these situations. Also, this example illustrates that one should use caution when trying to associate a brighter area in the MBRIS method with an elevated concentration of indigo.

If the imaging was performed again, a different backdrop (a board instead of a fabric) would be used to better contrast the object from the background. Also, the images indicate that the left side may be more exposed than the right side; making sure that the amount of light was even across the object would be important in future work.

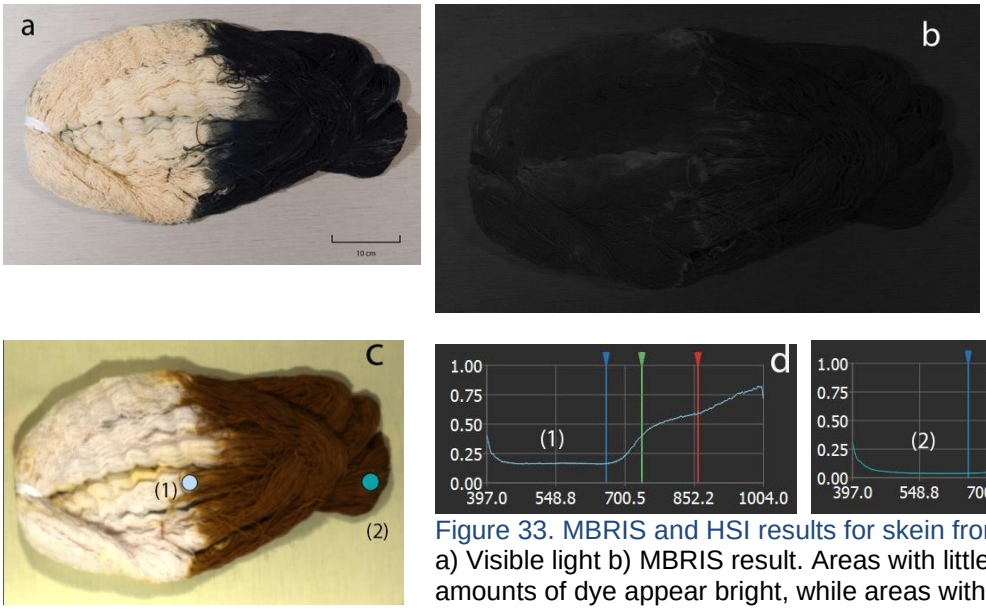

Figure 33. MBRIS and HSI results for skein from Mali (X90-271) a) Visible light b) MBRIS result. Areas with little to intermediate amounts of dye appear bright, while areas with high concentration of dye do not c) False-color hyperspectral image with RGB channels set to 862, 740, 660 nm, respectively d) Spectrum (1) e) Spectrum (2)

5.4.3 Jaina-style figurines (X91-2253 and X91-2269)

5.4.3.1 FORS

FORS analysis (Table 10) of the blue areas on two Jaina-style figurines (Figure 34) produced spectra (Figure 35) that were consistent with the presence of Maya blue; such features include reflectance maxima in the visible region at ~430 nm and ~530 nm with a small absorption at ~495 nm, followed by a major absorption maxima at ~665 nm and a steep rise to reflection. These spectra were compared to measurements taken on areas free of the blue material to ensure that the signals were due to the colorant

Table 10. Jaina-style figurines FORS data.

Sample name & [spectrum]	Blue colorant present?	λ_{ref}max (nm)	λ_{abs}max (nm)	λ_{inf} (nm)	Secondary absorptions (nm)
X91_2253_0 [0]	no	--	--	~566	1444, 1933, 2223
X91_2253_1 [1]	yes	433, 533	667	746	495, 1419, 1937, 2215
X91_2269_0 [2]	yes	440, 540	668	723	496, 1338, 1421, 1920, 2221
X91_2269_3 [3]	no	--	--	~568	1332, 1413, 1914, 2306
Maya blue (Kremer) [G]	--	430, 530	660	764	*~490*, 1417, ~1918, ~2220

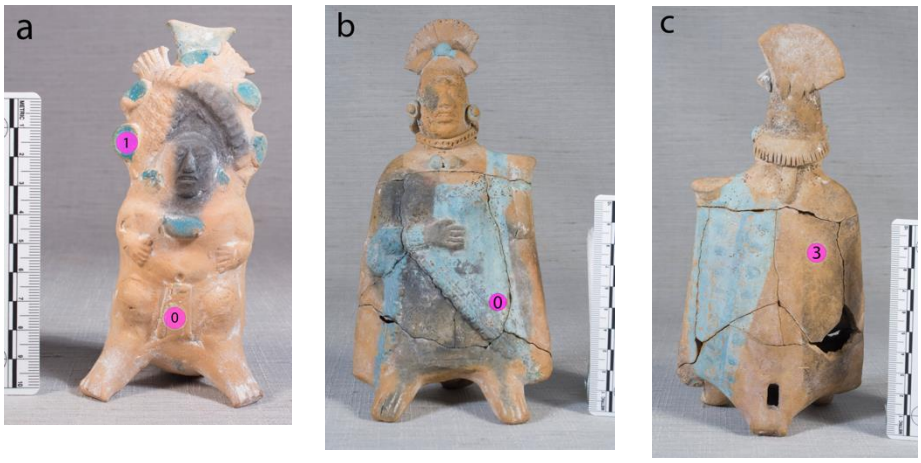

Figure 34. Jaina-style figurines, FORS measurement locations
a) X91-2253, obverse b) X91-2269, obverse C) X91-2269, reverse.

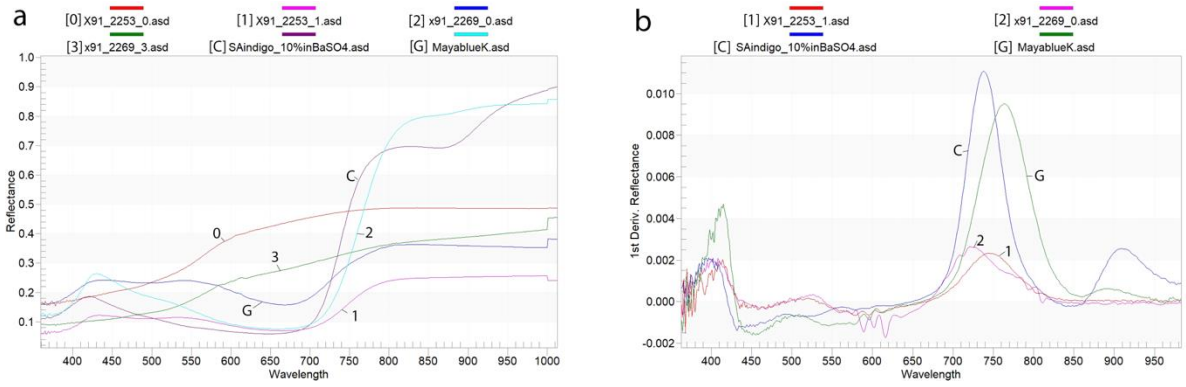

Figure 35. Jaina-style figurines reflectance spectra.
a) From areas with [1] and without [0] blue colorant on X91-2253, areas with [2] and without [3] blue colorant on X91-2269 b) First derivative shows that blue areas have $\lambda_{abs}max$ and λ_{inf} consistent with Maya blue.

5.4.3.2 MBRIS

As expected from the FORS results and MBRIS on Maya blue reference samples, the blue areas on the Jaina figurines appear bright relative to the rest of the object with the MBRIS method (Figure 36a-c).

When the reverse of X91-2269 was imaged with the MBRIS method, the blue garment (Figure 36d) draped across the figure's proper left shoulder appears bright. Within this brighter area, further details can be resolved (Figure 36e): a vertical stripe down the middle of this area with evenly-spaced short markings on either side of it appear even brighter. These features are

hard to resolve in the visible light image. The MBRIS method, in this case, provides enhanced visualization of the patterning executed in Maya blue on this part of the figurine. Whether this difference in appearance in the MBRIS is the result of multiple layers of colorant is an area worthy of further exploration. Building on this point, it would be worth studying how factors such as orientation of a three-dimensional object toward the photographic plane and light sources, wear, and fading affect MBRIS results.

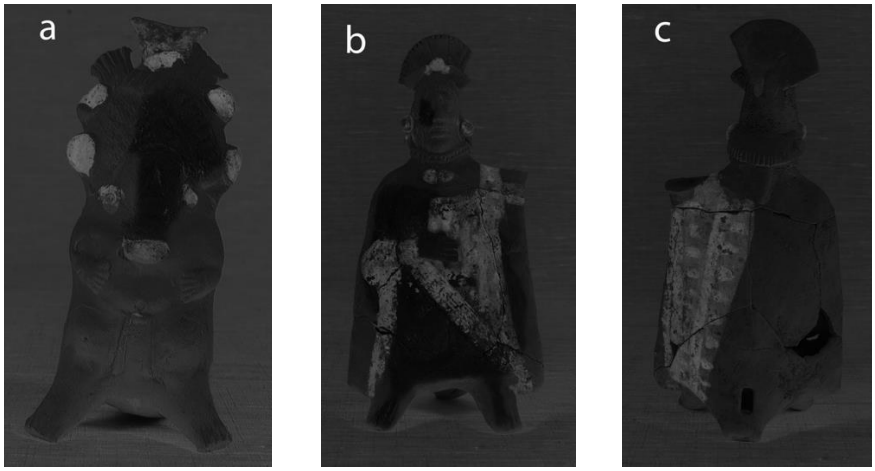

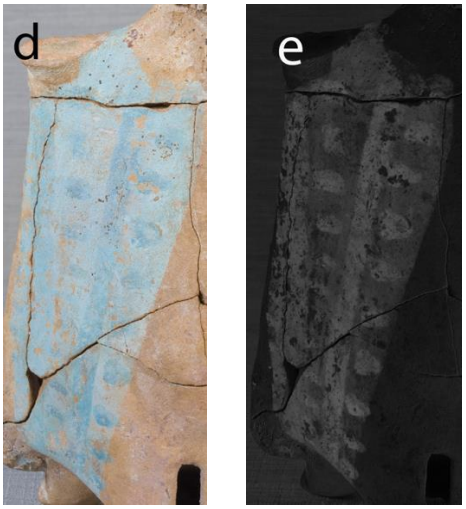

Figure 36. MBRIS results for Jaina-style figurines. Blue colorant appears bright. a) X91-2253, obverse b) X91-2269, obverse c) X91-2269, reverse d) X91-2269 reverse detail e) same area, MBRIS result.

5.4.3.3 HSI

In the false-color images (Figure 37) generated by the Specim IQ Studio software, the areas with Maya blue appear golden when the RGB channels are set to 860, 740, and 660 nm respectively. This result is consistent with the appearance of indigo-containing colorants in the

other false-color images created using the same wavelength bands.

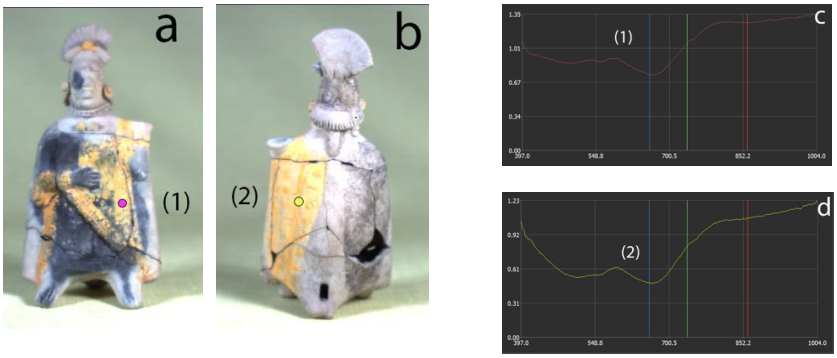

Figure 37. HSI on the Jaina-style figurine X91-2269.
a-b) False color hyperspectral images with RGB channels set to 860, 740 and 660 nm respectively c-d) Spectra from spots that contain blue colorant.

5.4.4 Comparisons

To further explore the behavior of indigo and Maya blue in the MBRIS results, two objects (X91.2269 and X2011.31.34) were placed in the same frame, along with pressed pellets of powdered colorants (BC indigo, Maya blue, smalt, and cobalt cerulean) (Figure 38a). As expected from the individual imaging experiments, the MBRIS result (Figure 38b) shows that both indigo on a textile and Maya blue on a ceramic appear bright relative to the rest of the objects. Thus, MBRIS does not distinguish between the two colorants; this is no surprise as it did not distinguish between the pure powder samples. As seen with the powders, the smalt and cobalt cerulean pellets appear brighter than the indigo and Maya blue pellets. This MBRIS result illustrates that the strength of the MBRIS method is providing a visual map of the location of a colorant that behaves in a way consistent to indigo or cobalt. This result also illustrates the limitations of attempting material identification with the MBRIS method alone.

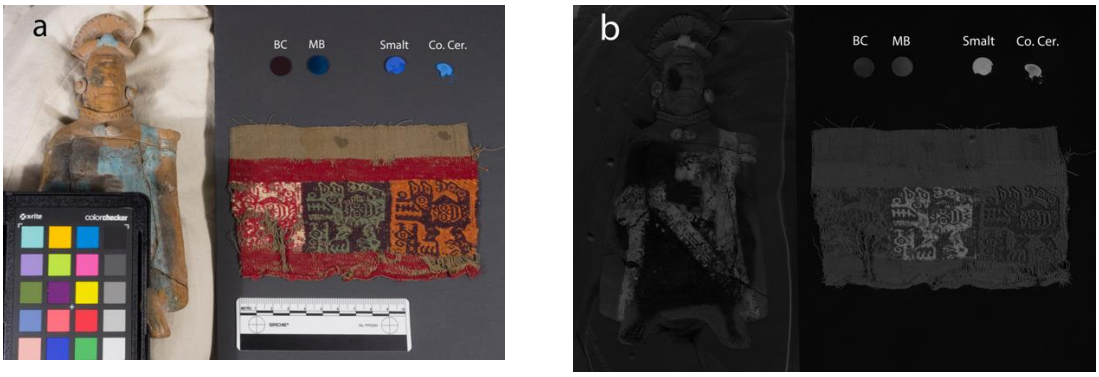

Figure 38. Comparison test with X91-2269, X2011.31.34, and pellets of powdered colorants from left to right: BC indigo, Maya blue, smalt, and cobalt cerulean.
a) Visible light, imaging setup b) MBRIS result. Indigo- and cobalt-containing pellets stand out from rest of image.

Indigo and Maya blue are considered different pigments, even if the latter contains the former as a main component. Distinguishing these two distinct pigments is possible with FORS, but both colorants appear bright in the MBRIS results. When reflectance spectra from the elements of Figure 38 are compared (Table 11) (Figure 39), the differences are subtle. Features present in Maya blue's spectrum and absent in indigo's include the small absorption at ~490 nm, narrowed main absorption band at ~660 nm, and absorptions in the NIR at ~1420 nm and 2220 nm from the clay component of the pigment. These differences are, of course, easier to observe on powdered reference samples compared to artifacts, where there is contribution from substrates and other materials.

Table 11. Comparison of FORS data from X91-2269 and X2011.31.34.

Sample name & [spectrum]	**λ_{ref} max (nm)**	**λ_{abs} max (nm)**	**λ_{inf} (nm)**	**Secondary absorptions (nm)**
BC, 100% [B]	419	~600	744	~860
BC, 10% in BaSO4	420	671	740	
Maya blue (Kremer) [G]	430, shoulder at 530	660	764	*~490*, 1417, *1673*, 1918, 2220, *2256*
X91_2269_0 [2]	440, 540	668	723	496, 1338, 1421, 1920, 2221
X_2011_31_34_probe0 [P0]	~526	652	716	

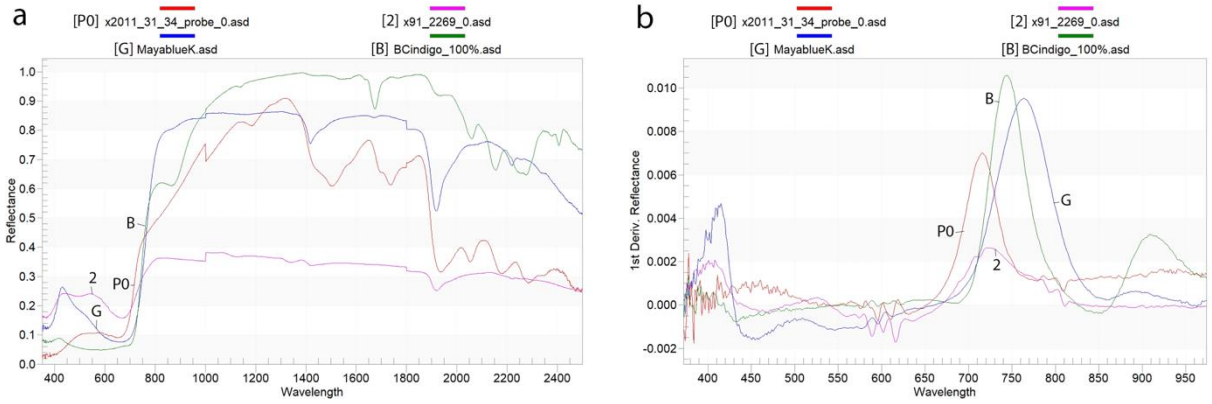

Figure 39. Reflectance spectra from samples and objects in Figure 38.
a) in the visible region, [P0] and [B] show good correlation and are distinguishable from [2] and [G]. b) First-order derivative.

False-color MBRIS

In the false-color MBRIS image (Figure 40), the Maya blue on the Jaina-style figurine and the green threads on the textile appear orange to golden. The pellets of BC indigo and Maya blue also appear faintly orange, unlike the smalt and cobalt cerulean pellets, which appear yellow to yellow-green. Thus, the false-color MBRIS result provides better visual differentiation than the grayscale MBRIS result.

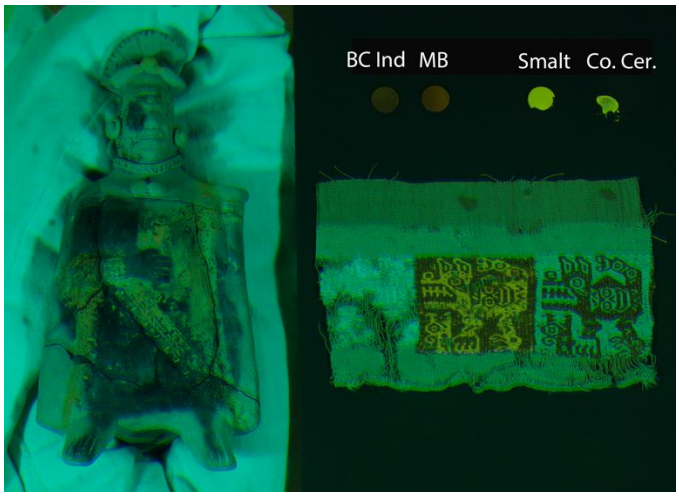

Figure 40. False-color MBRIS image of X91-2269, X2011.31.34, and pellets.
Areas with indigo appear golden orange, while the cobalt-containing pellets appear yellow.

The false-color image generated by the Specim IQ Studio software (Figure 41a), with the RGB channels set to 860, 740, and 660 nm respectively provided some unexpected results.

While the areas on the objects believed to contain indigo (Figure 41b) and Maya blue appeared golden, the pressed pellets of indigo and Maya blue appeared red. The BC indigo pellet may have been contaminated; the spectrum of from this pellet from the hyperspectral image (Figure 41c) is not consistent with spectral data collected from BC indigo with both the hyperspectral camera and FORS. The spectrum from the BC pellet has a small reflectance at ~690 nm, then an absorption at ~720 nm. These features are not present in the other spectral data collected from BC indigo.

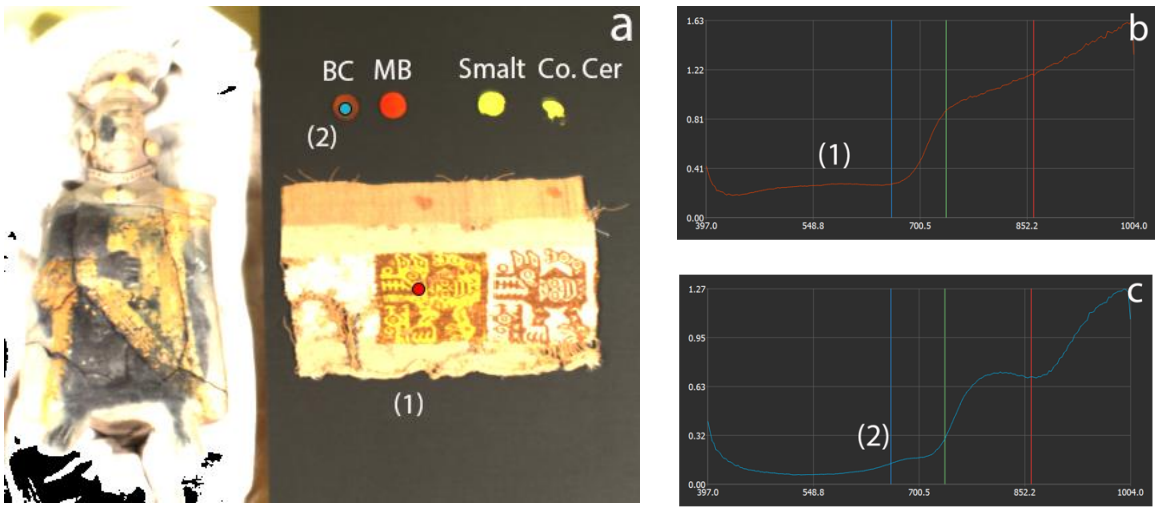

Figure 41. HSI on objects and samples from Figure 38.
a) False-color hyperspectral image with RGB channels set to 862, 740, 660 nm, respectively. Areas containing indigo on objects appear golden, while pellets containing indigo appear red-orange b) Spectrum from indigo-containing area marked on textile c) Spectrum from BC indigo pellet.

5.4.5 Balinese paintings (X2006.19.1 and X2006.19.2)

A 2009 study of these paintings as part of the UCLA/Getty Master's Program in the Conservation of Archaeological and Ethnographic Materials, under the supervision of Ioanna Kakoulli and Christian Fischer, sought to identify colorants using multiband imaging, FORS, and XRF. From the previous study, no indigo was identified as being present in either painting. The FORS data discussed for these paintings were collected during the previous study.

5.4.5.1 Balinese painting X2006.19.1

In the previous study, the blue colorant was identified as phthalo blue via FORS (Table

12) and XRF analysis. Spectra from blue areas (Figure 42) of the painting exhibit reflectance maxima at 473 nm and 492 nm, followed by a broad absorption band with two maxima absorptions at ~620 nm and ~700 nm. These features are not an exact match to the spectra from the reference phthalo blue; however, combined with the fact that copper was detected in XRF analysis, the blue colorant can confidently be identified as phthalo blue. The stratified nature of the painting and the fact that there are likely other colorants (i.e. white) present in the blue areas no doubt affect the FORS results.

Table 12. X2006.19.1 FORS data.

Sample name & [spectrum]	**Description**	**λ_{ref}max (nm)**	**λ_{abs}max (nm)**	**λ_{inf} (nm)**	**Secondary absorptions (nm)**
X2006_19_1_LRQS3 [3]	Blue skirt	473	615, 696	796	*~420, 1108*
X2006_19_1_URQS5 [5]	Blue water	492	625, 699	756	*~420*
X2006_19_1_LLQSJ7 [7]	Bright green structure	530	611, 676	696	1486
X2006_19_1_LLQSJ9 [9]	Bright green foliage	530	619, 678	695	1486
Phthalo (Kremer) [Q]		461	554, 677	856	*~420, 917, 1029,* 1105, 1680

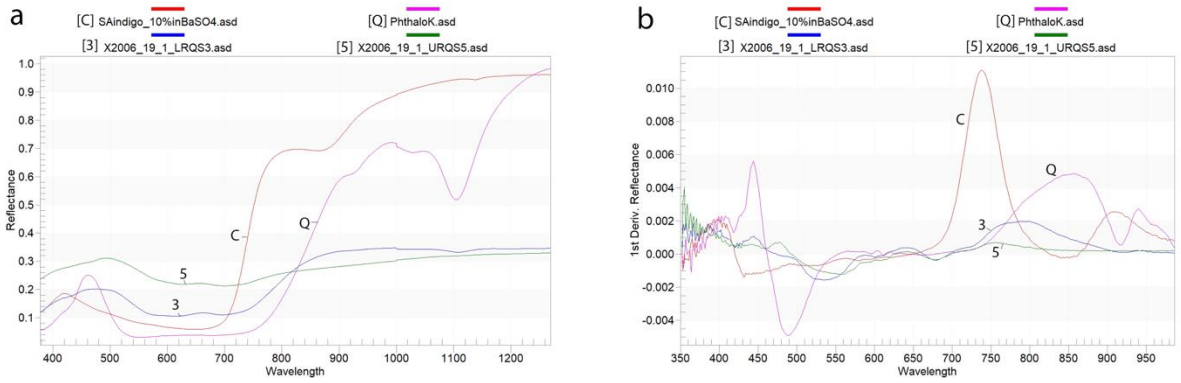

Figure 42. X2006.19.1 reflectance spectra, blue areas.
a) Comparison of reference phthalo blue to blue skirt [3] and blue water [5]. Spectra share λ_{ref}max at 460-490 nm, followed by a broad absorption band and rise to reflectance beginning at ~700 nm b) First derivative shows that rise to reflectance for blue areas and phthalo blue occurs at longer wavelengths compared to indigo.

The spectra from the blue areas of the painting as well as that from the reference

phthalo blue exhibit a rise to reflectance that begins at ~700 nm. The 660 nm BP and 735 nm BP filters do not adequately capture the transition from absorption to reflectance for this colorant; this is why the reference phthalo blue does not appear bright in the MBRIS result (Figure 16b). It is no surprise, then, that the blue areas of X2006.19.1 (Figure 43a) do not appear as bright when the MBRIS method is used (Figure 43b).

Figure 43. X2006.19.1, detail of blue skirt (LRQS3).
a) Visible light b) MBRIS result, blue skirt does not appear bright.

In the MBRIS result, however, areas with bright green colorant (Figure 44a) appear bright (Figure 44b). In the left foreground, for example, the structure (LLQSJ7) carried by some of the figures as well as the foliage (LLQSJ9)—executed in bright green colorant—appear bright in the MBRIS result. The colorants present in these bright green passages were not identified in the previous study, but spectra from these areas were collected.

FORS analysis on these bright green areas (Figure 45) revealed that they have reflection maxima at 530 nm, a double absorption at ~615 nm and 680 nm, followed by a rise to reflection that begins at ~680 nm with an inflection point at ~695 nm. Given these spectral features, It is thus no surprise that these green areas appear bright in the MBRIS result. Because the transition from absorption to reflection occurs at shorter wavelengths for this green colorant, the transition is captured by the MBRIS method, like it is for indigo. More analysis is required to identify this green colorant. Its reflectance profile resembles that of the blue areas

with the exception of shifts in the visible region to the major reflectance and absorptions; thus, it could be phthalo green or a mixture of the blue colorant and a yellow.

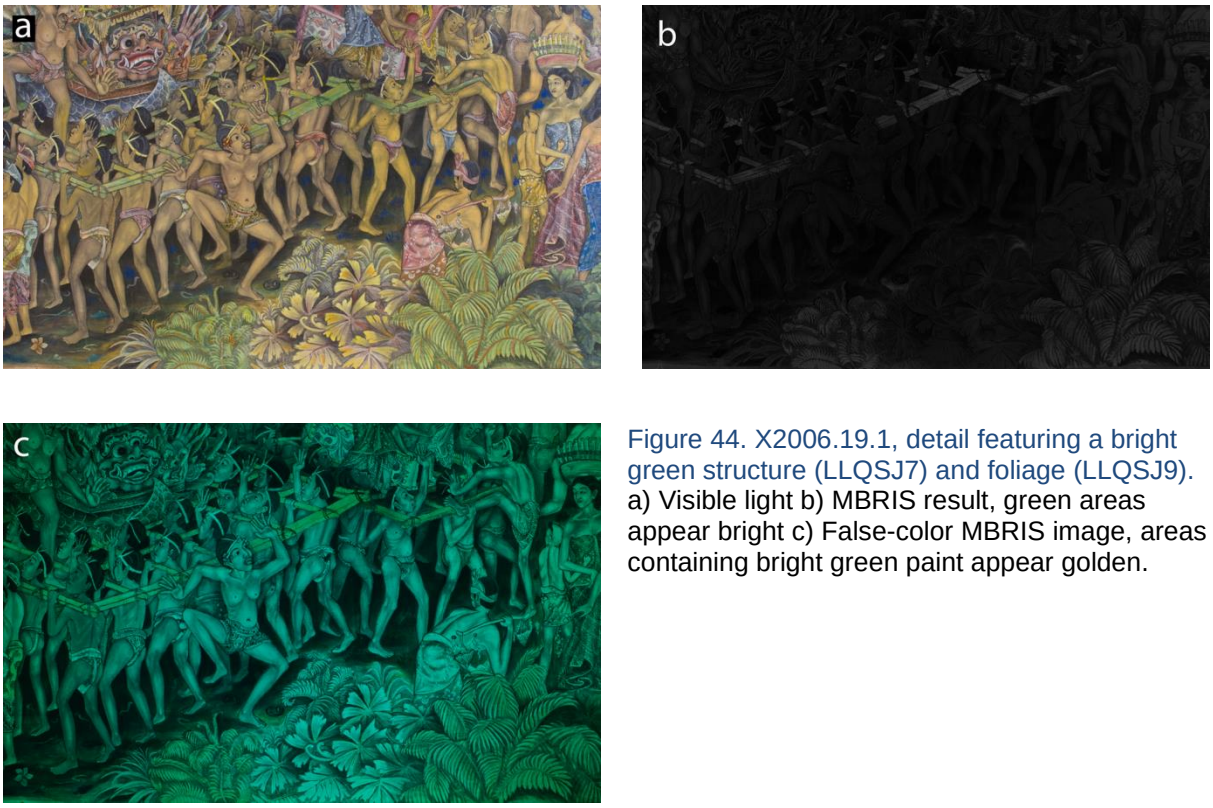

Figure 44. X2006.19.1, detail featuring a bright green structure (LLQSJ7) and foliage (LLQSJ9). a) Visible light b) MBRIS result, green areas appear bright c) False-color MBRIS image, areas containing bright green paint appear golden.

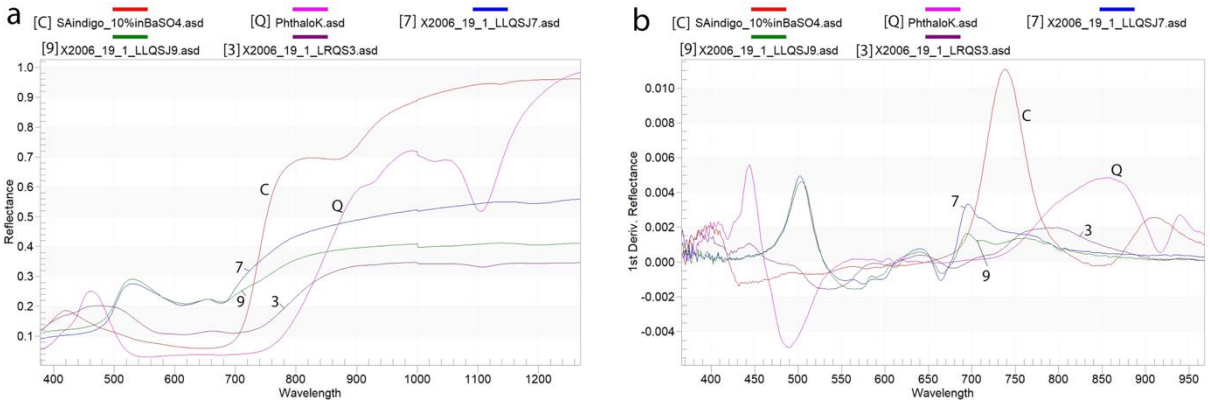

Figure 45. X2006.19.1 reflectance spectra, green areas.
a) Blue and bright green areas compared to phthalo blue and indigo references b) Rise to reflectance and inflection points for green areas occurs close to those for indigo.

In the false-color MBRIS image of this area (Figure 44c), the bright green features appear golden. This result demonstrates a shortcoming of the MBRIS false-color method: the

golden orange result in the false-color image is not unique to indigo. Even though the indigo-containing colorants were the only that appeared golden orange in the study of the powders, there are many other factors that make analysis of a painting more complicated, such as mixtures of pigments, a stratified structure, and presence of binding media.

5.4.5.2 Balinese painting X2006.19.2

In the 2009 study, the blue areas in this painting were found to contain ultramarine blue (Table 13). While the locations of the reflectance maxima vary, two spectra (LLQS4 and ULQS0) (Figure 46) clearly exhibit ultramarine's symmetrical absorption band with maximum at ~600 nm (Aceto et al. 2014).

The spectrum from the blue panel of the umbrella (URQSJ9) exhibits unique features in its main absorption band: instead of being smooth and symmetrical like LLQS4 and ULQS0, there are maximum absorptions at 537 nm, 560 nm and a small absorption at ~610 nm before rising to reflectance.

Table 13. X2006.19.2 FORS data.

Sample name & [spectrum]	Description	λ_{ref}max (nm)	λ_{abs}max (nm)	λ_{inf} (nm)	Secondary absorptions (nm)
X2006_19_2_LLQS4 [4]	Water in stream	506	606	676	--
X2006_19_2_ULQS0 [0]	Mountain	472	591	690	--
X006_19_2_URQSJ9 [J9]	Blue panel of umbrella	460	537, 560	696	*~610*
Lapis lazuli (Kremer)		463	595	714	*~810-825*
Ultramarine Light (Kremer) [M]		445	598	711	

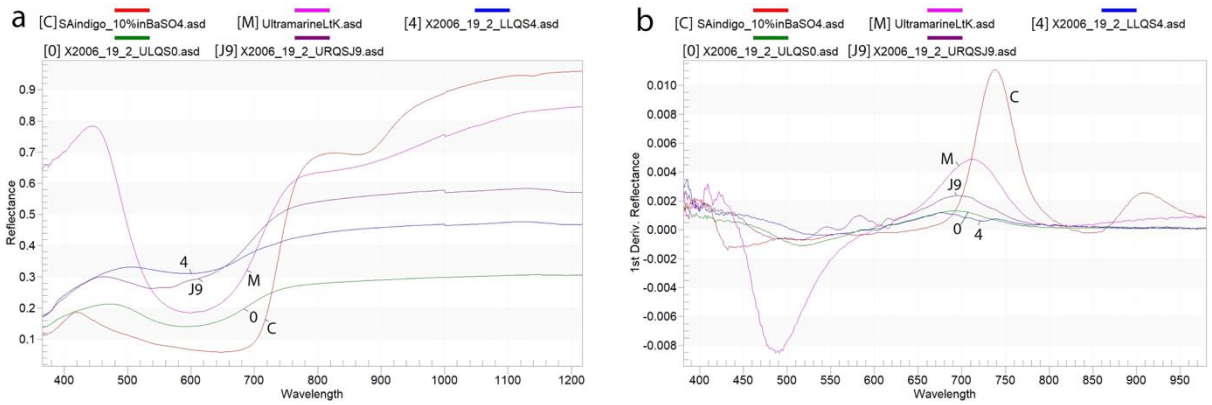

Figure 46. X2006.19.2 reflectance spectra.
a) Blue areas compared to reference ultramarine and indigo b) First derivative shows that rise to reflection and inflection points for blue areas occurs at shorter wavelengths than for indigo.

As noted earlier, powdered ultramarine and lapis lazuli samples appeared moderately bright in the MBRIS result; this is because the bandpass filters capture some of the transition from absorption to reflectance. As expected, many of the blue areas in X2006.19.2 (Figure 47a-b)—such as the blue panel of the umbrella, and the water in the stream in the foreground--appear brighter than the surrounding areas in the MBRIS result (Figure 47c-d).

As with X2006.19.1, the areas that appear bright in the MBRIS result appear golden in the false-color MBRIS images (Figure 47e-f). This is further confirmation that the golden orange result in the false-color image is not unique to indigo.

Figure 47. X2006.19.2, MBRIS and false-color MBRIS results of details featuring blue areas.
a) Foreground water (LLQS4), visible light b) Umbrella (URQSJ9), visible light c) Foreground water, MBRIS result d) Umbrella, MBRIS result e) Foreground water, false-color MBRIS image f) Umbrella, false-color MBRIS image.

5.4.5.3 Summary

The study of these two paintings illustrates that colorants other than indigo can appear bright relative to the rest of the work with the MBRIS method and can appear golden orange in the MBRIS false-color image. Reflectance spectra of these areas clearly revealed that the colorants standing out in the MBRIS results were not the same in both paintings—and that neither of them were indigo.

Context images of both paintings (Appendix C, Figure 54a-b) produced poor quality and potentially misleading overall MBRIS results (Appendix C, Figure 54c-d). Both MBRIS context images exhibited a dark center and bright edges. One explanation is that photographing the large object at a relatively close distance causes perspectival distortion that causes misalignment between the two bandpass images and thus affects the MBRIS result. Another possible explanation for this is that the work was not evenly lit; the light on either side of the painting creates a hot spot, leaving the center dark.

5.5 Fluorescence

This study sought to probe the fluorescence of indigo as a potential tool for non-invasive identification. Luminescence is a powerful tool that has been used to detect and map other colorants, like Egyptian blue, in cultural heritage (Kakoulli et al. 2017; Accorsi et al. 2009; Verri 2009).

5.5.1 FORS

In this research, the first attempt to probe the luminescence of indigo was using an alternative light source and the FORS instrument. The goal of this experiment was to replicate the previously published luminescence peak at ~750 nm (Clementi et al. 2009).

Overall, attempts to replicate the results published by Clementi et al. with this setup were not successful. A very weak peak may have been observed in some of the spectra at ~750 nm, but it was not clear whether this was coming from the sample or from the instrumental setup.

When a 10 w% by mass mixture of S-A indigo in barium sulfate was illuminated with UV radiation (bandwidth 310-390 nm, λ_{max} = 365 nm) and the instrument probe was placed as close to the sample as possible without touching it, a very small peak was possibly observed around 750 nm when the integration time was manually increased to 136 ms (Figure 48). However, tests with the same setup on the Spectralon® white reference (as a blank control) showed a

broad bump between ~625-800 nm that was not explained. Thus, results from the sample in this region should not be trusted.

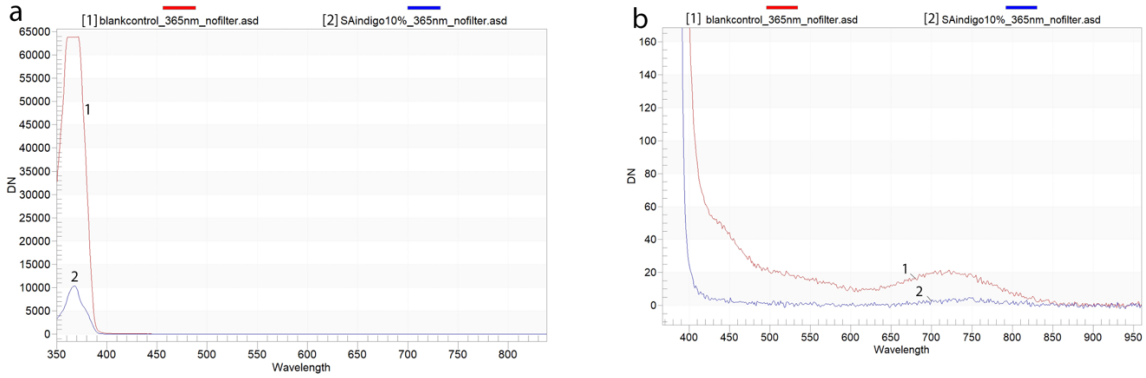

Figure 48. UV excitation emission spectra.
a) 10% S-A indigo in barium sulfate illuminated with UV radiation (λ_{max}=365 nm) b) Detail of a) showing broad bump from blank control (Spectralon®).

When a 10 w% mixture of S-A indigo in barium sulfate was illuminated with yellow light (λ_{max} = 575 nm) and the FORS probe was placed close to the sample, the result was similar to the test with UV excitation. In some of the measurements, a tiny peak around 750 nm may be present, but this required a long integration time (136 ms) (Figure 49). Again, there was evidence that this could be an artifact from the setup because measurements from the Spectralon® showed a broad bump between ~700-1000 nm. Yellow light was used because it was the closest bandwidth to the maximum absorption of indigo but did not pose the risk of interfering with the expected emission at 750 nm.

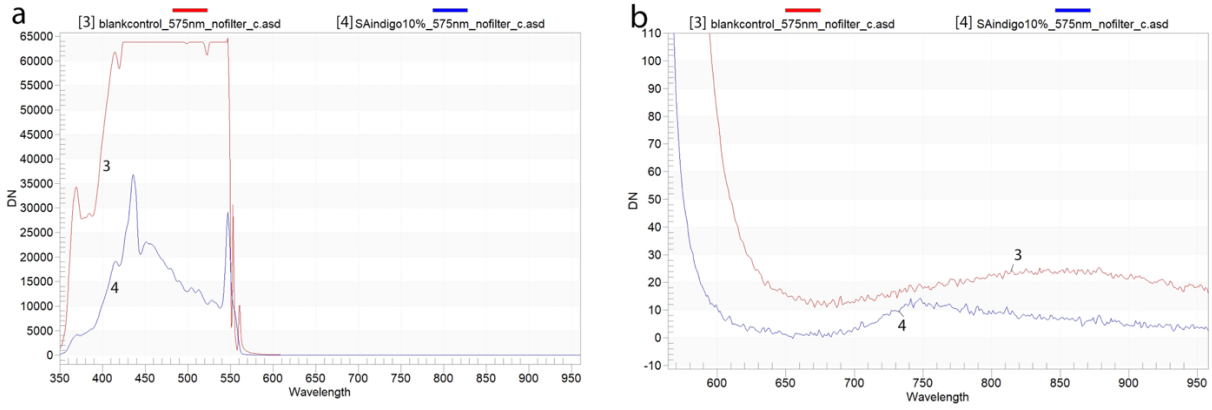

Figure 49. 575 nm excitation emission spectra.
a) 10% S-A indigo illuminated with yellow light (λ_{max}=575 nm) b) Detail of a) showing small reflectance peak at ~750 nm for indigo sample and broad bump for blank control.

It should be stressed that these “peaks” are extremely small (DN=15). In order to observe the peaks and bumps in this section, the scale at which the spectra were viewed was dramatically zoomed in compared to the reflectance studies. Thus, the conclusion was made that the experimental setup was not sensitive enough to detect the emission, which is documented by as being subtle to begin with. Thus, the decision was made to use other instrumentation to attempt to replace this peak at 750 nm.

5.5.2 Indigo in solution

Indigo would not be encountered on an artwork in solution; the end goal of this experimentation would be to work on a solid state sample. However, experiments on indigo in solution were conducted to see whether the instrumentation could detect the emission.

Measurements to characterize the maximum absorptions for solutions (Table 14, Figure 50) were as follows: 617 nm for S-A indigo (0.01 w% in DMSO), 620nm for BC indigo (0.01 w% in DMSO), and 623 nm for Maya blue (0.02 w% in DMSO). The measurement for the S-A indigo is consistent with the 619 nm value published by Pina et al. 2017. All of these values are blue-shifted compared to the maximum absorptions of the reference samples in solid state.

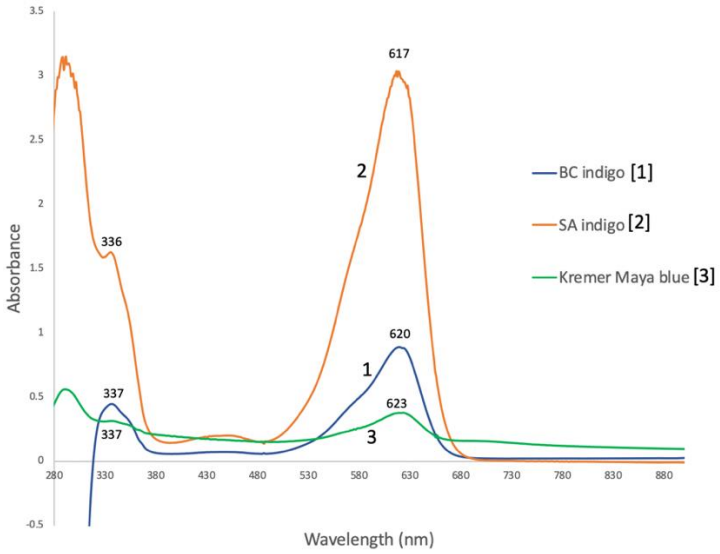

Figure 50. Absorbance measurements of indigo and Maya blue solutions in DMSO.
Solutions prepared at 0.01 w%, except for Maya blue, which was prepared at 0.02 w%.

An Ocean Optics spectrometer was used to measure fluorescence of the same solutions (Table 14, Figure 51). When excited with a yellow LED bulb (maximum emission at ~590nm), emissions were observed at ~670 nm. The sample was excited with a yellow LED bulb with maximum emission at 590nm. The emission of indigo solutions was observed at ~670 nm. This result required increasing the integration time to 30 seconds. This is consistent with the emission of S-A indigo in DMSO at 665 nm reported in Pina et al. 2017. A solution of Maya blue was also prepared and showed an even weaker emission at ~660-671 nm.

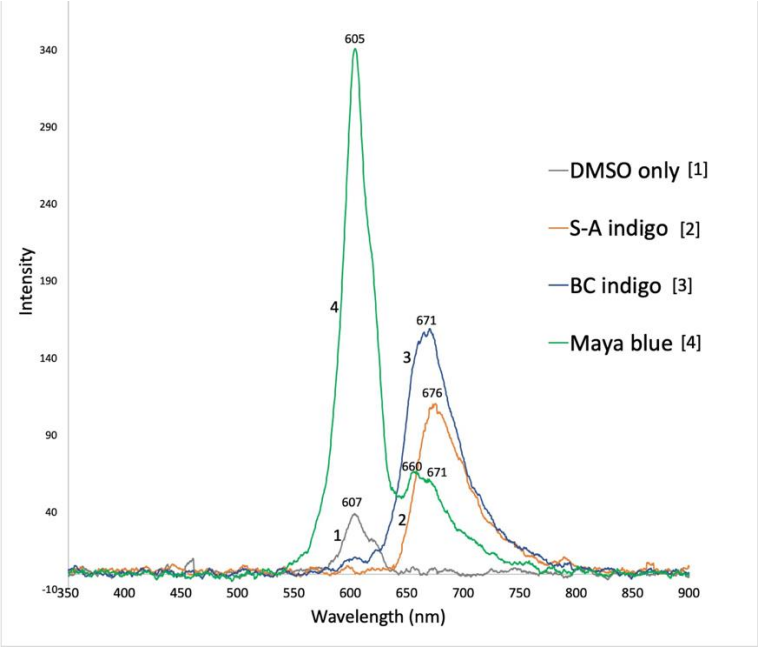

Figure 51. Fluorescence emissions of solutions prepared at 0.01 w% in DMSO.
The emission at ~605 nm is the light source.

Table 14. Absorption and emission results from solutions.

Solution in DMSO	λ_{abs}max (nm)	λ_{em}max (nm)
S-A indigo	617	676
BC indigo	620	671
Maya blue	623	~660-671

5.5.3 Solid State

After successfully detecting the emission in solution, the next experiments were conducted on solid samples (powder and dyed fiber) with the same light source and spectrophotometer.

However, detecting emission at ~750 nm was unsuccessful with this setup. The resulting spectra (Figure 52) showed a huge peak from the light source, but nothing at ~750 nm. A 600 nm long pass filter (cuts out radiation below 600 nm) was used to attempt to cut out some of this radiation, but still nothing appeared in the expected region around ~750 nm. There was a broad bump at ~825-925 nm in some of the measurements, but this feature was also observed on blank control tests. Because no emission was visible, it was suspected that the lack of results could be due to the fact that the fluorescence behavior of indigo is weak, with a quantum yield of ~0.002 (Pina et al. 2017). Thus, the same solid state setup was attempted with a sample of Egyptian blue, a pigment known to fluoresce with a higher quantum yield of 0.11 (Accorsi et al. 2009). Still no emission was observed; this indicates a problem with the experimental setup, but the source of the problem could not be determined. This solid state setup is not frequently used and thus troubleshooting it was difficult.

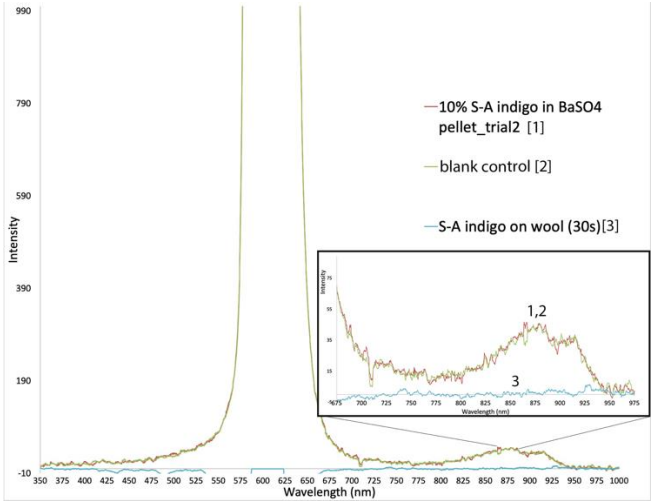

Figure 52. Fluorescence emissions of solid state experiments.
No emission attributed to indigo was detected.

6 Conclusions

The reexamination and evaluation of various spectroscopic and imaging techniques used by museum professionals for the characterization of indigo in cultural heritage materials has yielded interesting results. This MA research has confirmed the unbiased identification of the pigment using established spectroscopic techniques and has yielded new insights.

The analysis of indigo using FORS (from the UV through the NIR) provided fingerprint identification of the colorant regardless of the binding medium or chemical environment in which it is found. While the pigment's unbiased identification is ensured by the electronic transitions in the visible, the small absorption at ~860 nm observed in some of the indigo samples, has not been noted previously in published literature. This feature is worth further investigation as another possible characteristic absorption of indigo; its presence seems to be concentration dependent.

The reflectance spectra of indigo as a dye on a fiber substrate compared to those from indigo samples in powder form did not exhibit major differences. The differences observed appeared to mostly be a result of the concentration of the dye on the fiber substrate; spectra from dyed samples with higher concentrations of dye resemble the powdered indigo, while measurements on samples with lower concentrations of indigo exhibited a narrowed absorption band. Silk samples with low concentrations of indigo exhibited blue shifted main absorption bands.

While FORS was able to unequivocally differentiate amongst the different blue colorants that were part of this study, the MBRIS method (Webb, Summerour, and Giaccai 2014) was not. The MBRIS method failed to differentiate among indigo, Maya blue, cobalt-containing pigments, and lapis lazuli or ultramarine). As such, the MBRIS method cannot identify and map indigo without the aid of additional analytical techniques. Furthermore, as one case study (X2006.19.1) illustrated, the MBRIS method can also give false-positives for green colorants. Additionally, as

illustrated by one case study (X90-271), the MBRIS method was not successful in mapping indigo for areas in which the colorant was highly concentrated.

While this research acknowledges the potential of MBRIS as a macroscale imaging technique to map the spatial distribution of indigo across the surface being imaged, a significant shortcoming is its inability to differentiate indigo from other blue (and green) colorants. Thus, without the use of complementary spectroscopic techniques, the MBRIS method result mean little without the aid of cultural context and additional analytical techniques.

A new method utilizing principles of the MBRIS method is based on the development of composite trichromatic false-color images using the MBRIS result together with the two bandpass (660 nm and 735 nm) images. The resulting false-color images showed a greater level of differentiation between indigo and other blue colorants in the powder form: those containing indigo were the only ones that appeared orange or golden. When applied to case studies, this method was less successful; as with the MBRIS result, false positives were given. These results suggest that the bands used in the MBRIS method are too broad to effectively differentiate some of the blue colorants—even when false-color images are employed.

Hyperspectral imaging spectroscopy in the visible and NIR, combined with trichromatic false-color imaging processing has shown promising results. HSI allowed spectral data to be collected across a large surface in a quick fashion. The combination of spectral and spatial information provides unbiased identification of the pigment; the created of false-color trichromatic images using specific bands (660 nm, 740 nm, 860 nm) from the spectral cube also allowed spatially resolved data visualization.

The fluorescence of indigo could only be detected in samples in solution. In solid samples, this emission was not detectable. This may be due to the experimental setup used in this study, or because the fluorescence is likely too weak to be recorded by luminescence imaging techniques commonly used to map other of colorants in the cultural heritage field, like Egyptian blue for example. The most current research (Pina et al. 2017) indicates that the

fluorescence quantum yield of indigo is over fifty times weaker than that of Egyptian blue. This weak fluorescence behavior seems to be best probed with a fluorimeter that is specifically designed to measure solid samples and for which excitation wavelength can be well-customized. Systematic research of this type into the fluorescence of indigo on a broad set of indigo reference samples as well as cultural heritage material containing indigo would be valuable.

7 Appendices

7.1 Appendix A: Additional information on reference powder samples

Table 15. Indigo and blue powder samples reference analyzed with FORS

Sample name		Description	Chemical Formula
[A]	SAindigo_100%	Sigma-Aldrich indigo (synthetic)	$C_{16}H_{10}N_2O_2$
[B]	BCindigo_100%	Botanical Colors indigo (natural), from *Indigofera tinctoria*	--
[C]	SAindigo_10%inBaSO4	Sigma-Aldrich indigo, 10 w% in BaSO4	$C_{16}H_{10}N_2O_2$
[D]	BCindigo_10%inBaSO4	Botanical Colors indigo, 10 w% in BaSO4	--
[E]	Jindigo_10%inBaSO4	Pre-reduced indigo from Jacquard Indigo Dye Kit	--
[F]	Kindigolake_10%inBaSO4	Kremer Pigments 36005, indigo blue lake (from *Indigofera tinctoria*, precipitated with aluminum hydroxide), 10 w% in BaSO4	$C_{16}H_{10}N_2O_2$ and $Al(OH)_3$
[G]	MayablueK	Kremer Pigments 36007, Maya blue	Indigo and palygorskite, $(Mg, Al)_4Si_8(O, OH, H_2O)_{24}.nH_2O$ (Leona et al. 2004)
[H]	SmaltK	Kremer Pigments 10000, smalt standard grind	Cobalt potassium silicate
[J]	CobaltCerK	Kremer Pigments 45730, cobalt cerulean blue	Cobalt tin oxide
[K]	CobaltMedK	Kremer Pigments 45710, cobalt blue medium	Cobalt aluminate spinel
[L]	LapisLazuliK	Kremer Pigments 10562, Lapis Lazuli, sky-blue	Sodium calcium aluminum silicate $(Na, Ca)_8[(SO_4,S,Cl)_2(AlSiO_4)_6]$
[M]	UltramarineLtK	Kremer Pigments 45080, Ultramarine blue, light	Sodium aluminum sulfo silicate
[N]	EgyptianK	Kremer Pigments 10060, Egyptian blue	Copper calcium silicate, $CaCuSi_4O_{10}$
[P]	HanK	Kremer Pigments 10071, Han blue fine, 0-40µ	Copper barium silicate, $BaCuSi_4O_{10}$
[Q]	PhthaloK	Kremer Pigments 23050, Phthalo Blue, primary	Copper phthalocyanine $C_{32}H_{15}N_8Cu$
[R]	HeliogenK	Kremer Pigments 23050, Heliogen® blue	Copper phthalocyanine $C_{32}H_{15}N_8Cu$
[S]	AzuriteK	Kremer Pigments 10200, azurite natural standard, 0-120µ	Copper hydroxide carbonate, $Cu_3(CO_3)_2(OH)_2$
[T]	PrussianK_10%inBaSO4	Kremer Pigments 45202 , 10 w% in barium sulfate	Ferric ferrocyanide $C_{18}Fe7N_{18}$
*all chemical formulas were obtained from technical data provided by Kremer Pigmente unless otherwise noted			

7.2 Appendix B: Additional data on paint swatches

Spectra from S-A and BC indigo paint swatches did not reveal major differences compared to the powdered colorants (Figure 53). No absorption at ~860 nm was observed in the indigo paint swathes. The BC indigo swatch had an inflection point that was slightly blue-shifted (to 730 nm) compared to the powdered BC indigo. This blue-shifted inflection point in the major transition from absorption to reflectance was also observed in the cobalt cerulean and cobalt medium swatches. However, as mentioned before, it is difficult to draw conclusions as many of the swatches did not product good quality spectra.

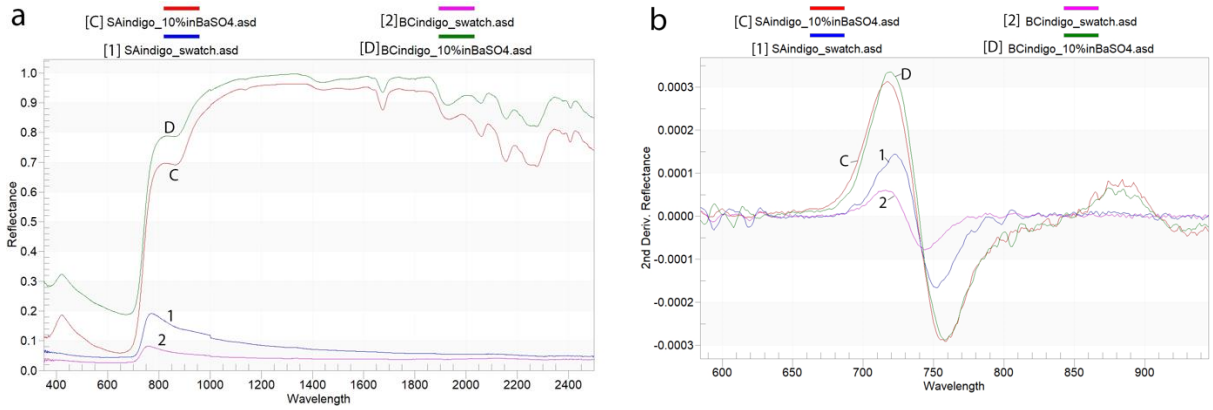

Figure 53. Indigo paints swatches reflectance spectra.
a) S-A and BC swatches share same major absorption and transition to reflectance as powdered samples b) Second derivative shows λ_{inf} for BC swatch is slightly blue-shifted compared to BC powder.

7.3 Appendix C: Overall images of X2006.19.1 and X2006.19.2

Figure 54. Overall images of X2006.19.1 and X2006.19.2.
a) X2006.19.1,visible light b) X2006.19.2, visible light c) X2006.19.1, MBRIS result d) X2006.19.2, MBRIS result

7.4 Appendix D: Materials used

Indigo:
Indigo (229296), Sigma-Aldrich, dye content 95%
Botanical Colors indigo (natural, from *Indigofera tinctoria*)
https://botanicalcolors.com/shop/natural-dye-extracts/organic-indigo/
Pre-reduced indigo, Jacquard Products https://www.jacquardproducts.com/indigo-tie-dye-kit

Kremer Pigments:
Indigo blue lake (36005)
Lapis Lazuli, sky-blue (10562)
Prussian blue (45202)
Azurite natural standard, 0-120µ (10200)
Cobalt cerulean blue (45730)
Maya blue (36007)
Han blue fine, 0-40µ (10071)
Smalt standard grind (10000)
Egyptian blue (10060)
Ultramarine blue, light (45080)
Heliogen® blue (23050)
Cobalt blue medium (45710)
phthalo blue (23050)
Pit lime (calcium hydroxide) (31800)

Fibers:
Baby llama chunky, 100% baby llama, Cascade Yarns
Organic cotton, Aurora Silk
Silk habutae, 8mm (609), Testfabrics, Inc.
Worsted wool challis (542), Testfabrics, Inc.

Other:
Barium sulfate (202762), Sigma-Aldrich
Dimethyl sulfoxide (D128-1), Fisher Chemical
Hydrosulfite, from dyeing kit manufactured by Jacquard Products
https://www.jacquardproducts.com/indigo-tie-dye-kit
Fructose, nuts.com https://nuts.com/cookingbaking/sweeteners/natural-sugar-replacements/fructose/1lb.html

Weighing paper, 3x3 in, Fisher Chemical
Weighing dish, 12ml, polystyrene, Fisher Chemical

8 References

Accorsi, Gianluca, Giovanni Verri, Margherita Bolognesi, Nicola Armaroli, Catia Clementi, Costanza Miliani, and Aldo Romani. 2009. “The Exceptional Near-Infrared Luminescence Properties of Cuprorivaite (Egyptian Blue).” *Chemical Communications* 23: 3392–94. https://doi.org/10.1039/b902563d.

Aceto, Maurizio, Angelo Agostino, Gaia Fenoglio, Ambra Idone, Monica Gulmini, Marcello Picollo, Paola Ricciardi, and John K. Delaney. 2014. “Characterisation of Colourants on Illuminated Manuscripts by Portable Fibre Optic UV-Visible-NIR Reflectance Spectrophotometry.” *Analytical Methods* 6 (5): 1488–1500. https://doi.org/10.1039/c3ay41904e.

Angelini, Luciana Gabriella, Sabrina Tozzi, Susanna Bracci, Franco Quercioli, Bruno Radicati, and Marcello Picollo. 2010. “Characterization of Traditional Dyes of the Mediterranean Area By Non-Invasive UV-Vis-NIR Reflectance Spectroscopy.” *Studies in Conservation* 55 (sup2): 184–89. https://doi.org/10.1179/sic.2010.55.Supplement-2.184.

Baeyer, Adolf, and Viggo Drewsen. 1882. “Darstellung von Indigblau Aus Orthonitrobenzaldehyd.” *Berichte Der Deutschen Chemischen Gesellschaft* 15 (2): 2856–64. https://doi.org/10.1002/cber.188201502274.

Balfour-Paul, Jenny. 1998. *Indigo*. Buffalo, NY: Firefly Books.

BASF. n.d. “Bringing Color to Life: Shade Card for Pigments for Packaging Inks.” BASF. file:///Users/megansalas/Downloads/141011_EDC_0914e_Bringing-Color-to-Life-web_FINAL.pdf.

Bernardino, N. D., V. R.L. Constantino, and D. L.A. De Faria. 2018. “Probing the Indigo Molecule in Maya Blue Simulants with Resonance Raman Spectroscopy.” Research-article. *Journal of Physical Chemistry C* 122 (21): 11505–15. https://doi.org/10.1021/acs.jpcc.8b01406.

Blackburn, Richard S., Thomas Bechtold, and Philip John. 2009. “The Development of Indigo Reduction Methods and Pre-Reduced Indigo Products.” *Coloration Technology* 125 (4): 193–207. https://doi.org/10.1111/j.1478-4408.2009.00197.x.

Bradley, Lauren, Jessica Ford, Dawn Kriss, Victoria Schussler, Federica Pozzi, Elena Basso, and Lisa Bruno. 2018. “Evaluating Multiband Reflectance Image Subtraction for the Characterization of Indigo in Romano-Egyptian Funerary Portraits.” Los Angeles: Appear: Ancient Panel Painting, Examination, Analysis and Research.

Clark, Robin J.H., Christopher J. Cooksey, and Marcus A.M. Daniels. 1993. “Indigo, Woad, and Tyrian Purple : Important Vat Dyes from Antiquity to the Present.” *Endeavour* 17 (4): 191–99.

Clementi, C., C. Miliani, A. Romani, U. Santamaria, F. Morresi, K. Mlynarska, and G. Favaro. 2009. “In-Situ Fluorimetry: A Powerful Non-Invasive Diagnostic Technique for Natural Dyes Used in Artefacts. Part II. Identification of Orcein and Indigo in Renaissance Tapestries.” *Spectrochimica Acta - Part A: Molecular and Biomolecular Spectroscopy* 71 (5): 2057–62. https://doi.org/10.1016/j.saa.2008.08.006.

Cosentino, Antonio. n.d. “FORS Spectral Database.” Cultural Heritage Science Open Source. Accessed June 5, 2020. https://chsopensource.org/fors/#BLUES.

Degani, Laura, Chiara Riedo, and Oscar Chiantore. 2015. “Identification of Natural Indigo in Historical Textiles by GC–MS.” *Analytical and Bioanalytical Chemistry* 407 (6): 1695–1704. https://doi.org/10.1007/s00216-014-8423-2.

Delaney, John K., Elizabeth Walmsley, Barbara H. Berrie, and Colin F. Fletcher. 2005. “Multispectral Imaging of Paintings in the Infrared to Detect and Map Blue Pigments.” In *Scientific Examination of Art: Modern Techniques in Conservation and Analysis*, 120–36. Washington, D.C.: National Academies Press.

Eduardo, Luiz, Carlos Roberto, and De Souza Filho. 2011. “Remote Sensing of Environment Identification of Mineral Components in Tropical Soils Using Reflectance Spectroscopy and Advanced Spaceborne Thermal Emission and Re Fl Ection Radiometer (ASTER) Data.” *Remote Sensing of Environment* 115 (8): 1824–36. https://doi.org/10.1016/j.rse.2011.02.023.

Fang, Qian, Hanlie Hong, Lulu Zhao, Stephanie Kukolich, Ke Yin, and Chaowen Wang. 2018. “Visible and Near-Infrared Reflectance Spectroscopy for Investigating Soil Mineralogy : A Review.” *Journal of Spectroscopy*.

Fischer, Christian. 2020. “Personal Communication.”

Fischer, Christian, and Ellen Hsieh. 2017. “Export Chinese Blue-and-White Porcelain: Compositional Analysis and Sourcing Using Non-Invasive Portable XRF and Reflectance Spectroscopy.” *Journal of Archaeological Science* 80: 14–26. https://doi.org/10.1016/j.jas.2017.01.016.

Fischer, Christian, and Ioanna Kakoulli. 2018. “UV-Vis-NIR Spectroscopy.” Los Angeles.

Fowler Museum. n.d. “X2006.19.1.” Los Angeles.

———. n.d. “X2006.19.2.” Los Angeles.

———. n.d. “X2011.31.34.” Los Angeles.

———. n.d. “X90.271.” Los Angeles.

———. n.d. “X91.2253.” Los Angeles.

———. n.d. “X91.2269.” Los Angeles.

Galaxy Scientific. 2018. “Chart of Near-IR Absorption Bands.” https://galaxy-scientific.com/news/chart-of-nir-absorption-bands-poster/.

“Indigo Instructions.” 2018. Botanical Colors. 2018. https://botanicalcolors.com/indigo-instructions/.

Jain, Anil K. 1989. *Fundamentals of Digital Image Processing*. Edited by Thomas Kailath. Englewood Cliffs, NJ: Prentice Hall.

Kakoulli, Ioanna, Roxanne Radpour, Yuan Lin, Marie Svoboda, and Christian Fischer. 2017. "Application of Forensic Photography for the Detection and Mapping of Egyptian Blue and Madder Lake in Hellenistic Polychrome Terracottas Based on Their Photophysical Properties." *Dyes and Pigments* 136: 104–15. https://doi.org/10.1016/j.dyepig.2016.08.030.

Kobayashi, T., and P.M. Rentzepis. 1979. "On the Picosecond Kinetics and Photostability of Indigo and 6,6′- Dimethoxyindigo." *Journal of Chemical Physics* 70 (2): 886–92.

Kremer Pigmente. n.d. "10000 & 10010 Smalt." Kremer Pigmente.

———. n.d. "23050 Phthalo Blue, Heliogen® Blue."

———. n.d. "45710 Cobalt Blue, Medium."

———. 2012. "10000 Smalt, Standard."

———. 2018a. "45710 Cobalt Blue Medium."

———. 2018b. "45730 Cobalt Cerulean Blue." Material Safety Data Sheet.

Kriss, Dawn, Lauren Bradley, Jessica Ford, Elyse Driscoll, and Victoria Schussler. 2019. "Materials Characterization with Multiband Reflectance Image Subtraction at the Brooklyn Museum: A New Tool for the Multiband Imaging Kit." *American Institute for Conservation 47th Annual Meeting, May 16, 2019*. Uncasville, CT. https://aics47thannualmeeting2019.sched.com/event/Iui6/imaging-toolstechniques-tactics-materials-characterization-with-multiband-reflectance-image-subtraction-at-the-brooklyn-museum-a-new-tool-for-the-multiband-imaging-kit.

Leona, Marco, Francesca Casadio, Mauro Bacci, and Marcello Picollo. 2004. "Identification of the Pre-Columbian Pigment Maya Blue on Works of Art by Noninvasive UV-Vis and Raman Spectroscopic Techniques." *Journal of the American Institute for Conservation* 43 (1): 39–54. https://doi.org/10.1179/019713604806112632.

Leona, Marco, and John Winter. 2001. "Studies in Conservation Fiber Optics Reflectance Spectroscopy : A Unique Tool for the Investigation of Japanese Paintings" 3630. https://doi.org/10.1179/sic.2001.46.3.153.

Matarazzo, Augusto, and Robert H. E. Hudson. 2015. "Fluorescent Adenosine Analogs : A Comprehensive Survey." *Tetrahedron* 71 (11): 1627–57. https://doi.org/10.1016/j.tet.2014.12.066.

Maugard, Thierry, Estelle Enaud, Patrick Choisy, and Marie Dominique. 2001. "Identification of an Indigo Precursor from Leaves of.Pdf" 58: 897–904.

McVicker, Donald. 2012. "Figurines Are Us? The Social Organization of Jaina Island, Campeche, Mexico." *Ancient Mesoamerica* 23: 211–34. https://doi.org/10.1017/S0956536112000168.

Miliani, C., A. Romani, and G. Favaro. 1998. “A Spectrophotometric and Fluorimetric Study of Some Anthraquinoid and Indigoid Colorants Used in Artistic Paintings.” *Spectrochimica Acta - Part A: Molecular and Biomolecular Spectroscopy* 54 (4): 581–88. https://doi.org/10.1016/S1386-1425(97)00240-0.

Monahan, Alan R., and James E. Kuder. 1972. “Spectroscopic Differences between Crystalline and Amorphous Phases of Indigo.” *Journal of Organic Chemistry* 37 (25): 4182–84. https://doi.org/10.1021/jo00798a048.

Perkin, F. Mollwo. 1900. “The Present Condition of the Indigo Industry.” *Nature* 63 (1618): 7–9.

Pina, J., Daniela Sarmento, Marco Accoto, Pier Luigi Gentili, Luigi Vaccaro, Adelino Galvão, and J. Sérgio Seixas De Melo. 2017. “Excited-State Proton Transfer in Indigo.” *Journal of Physical Chemistry B* 121 (10): 2308–18. https://doi.org/10.1021/acs.jpcb.6b11020.

Plesters, Joyce. 1966. “2. Ultramarine Blue, Natural and Artificial.” *Studies in Conservation* 11 (2): 62–75. https://doi.org/10.1179/sic.1966.009.

Pliny the Elder. n.d. *The Natural History*. Edited by John Bostock and H.T. Riley. 1855th ed. London: Taylor & Francis. http://data.perseus.org/citations/urn:cts:latinLit:phi0978.phi001.perseus-eng1:35.27.

Romani, Aldo, Catia Clementi, Costanza Miliani, and Gianna Favaro. 2010. “Fluorescence Spectroscopy: A Powerful Technique for the Noninvasive Characterization of Artwork.” *Accounts of Chemical Research* 43 (6): 837–46. https://doi.org/10.1021/ar900291y.

Seixas de Melo, J., A. P. Moura, and M. J. Melo. 2004. “Photophysical and Spectroscopic Studies of Indigo Derivatives in Their Keto and Leuco Forms.” *Journal of Physical Chemistry A* 108 (34): 6975–81. https://doi.org/10.1021/jp049076y.

Sigma-Aldrich. n.d. “Indigo.” Sigmaaldrich.Com. Accessed May 9, 2020. https://www.sigmaaldrich.com/catalog/product/aldrich/229296?lang=en&region=US.

Tsiantos, Constantinos, Maria Tsampodimou, George H. Kacandes, Manuel Sanchez del Rio, Vassilis Gionis, and Georgios D. Chryssikos. 2012. “Vibrational Investigation of Indigo – Palygorskite Association(s) in Synthetic Maya Blue.” *Journal of Materials Science* 47 (7): 3415–28. https://doi.org/10.1007/s10853-011-6189-x.

Verri, G. 2009. “The Spatially Resolved Characterisation of Egyptian Blue , Han Blue and Han Purple by Photo-Induced Luminescence Digital Imaging.” *Analytical and Bioanalytical Chemistry* 394: 1011–21. https://doi.org/10.1007/s00216-009-2693-0.

Webb, E. Keats, Rebecca Summerour, and Jennifer Giaccai. 2014. “A Case Study Using Multiband and Hyperspectral Imaging for the Identification and Characterization of Materials on Archaeological Andean Painted Textiles.” *AIC Textile Speciality Group Postprints* 24: 23–35.

Wyman, George M., and Julius Weinstein. 1956. “Spectroscopic Studies on Dyes. I. The Association of Indigo Dyes in the Solid Phase.” *Journal of the American Chemical Society* 78 (11): 2987–2390. https://doi.org/10.1021/ja01592a012.